Bioengineering Self-organizing Signalling Centres to Control Embryoid Body Pattern Elaboration

Bioengineering Self-organizing Signalling Centres to Control Embryoid Body Pattern Elaboration.

Authors: Fokion Glykofrydis[1,2*], Elise Cachat[3], Ieva Berzanskyte[1], Elaine Dzierzak[2] and Jamie A. Davies[1]

[1] UK Centre for Mammalian Synthetic Biology, Centre for Discovery Brain Sciences, The University of Edinburgh, Edinburgh, EH8 9XD, United Kingdom

[2] MRC Centre for Inflammation Research, The Queen's Medical Research Institute, The University of Edinburgh, Edinburgh, EH16 4TJ, United Kingdom

[3] UK Centre for Mammalian Synthetic Biology, Institute of Quantitative Biology, Biochemistry, and Biotechnology, The University of Edinburgh, Edinburgh, EH9 3BF, United Kingdom

[*] Corresponding author/Lead contact: Fokion Glykofrydis (s1316049@sms.ed.ac.uk)

For Table of Contents Use Only

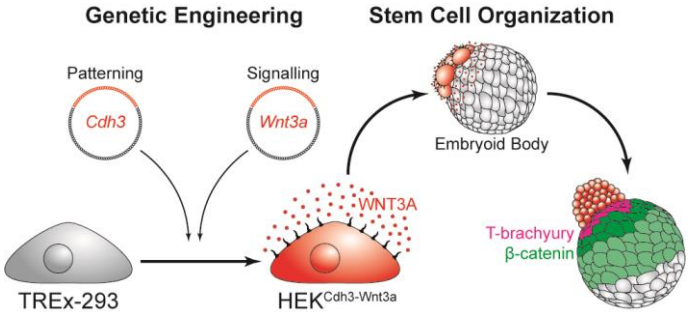

Abstract

Multicellular systems possess an intrinsic capacity to autonomously generate non-random state distributions or morphologies in a process termed self-organization. Facets of self-organization, such as pattern formation, pattern elaboration, and symmetry breaking, are frequently observed in developing embryos. Artificial stem cell-derived structures including embryoid bodies (EBs), gastruloids and organoids also demonstrate self-organization, but with a limited capacity compared to their *in vivo* developmental counterparts. There is a pressing need for better tools to allow user-defined control over self-organization in these stem cell-derived structures. Here, we employ synthetic biology to establish an efficient platform for the generation of self-organizing co-aggregates, in which HEK-293 cells overexpressing P-cadherin (*Cdh3*) spontaneously form cell clusters attached mostly to one or two locations on the exterior of EBs. These *Cdh3*-expressing HEK cells, when further engineered to produce functional mouse WNT3A, evoke polarized and gradual Wnt/β-catenin pathway activation in EBs during co-aggregation cultures. The localized WNT3A provision induces nascent mesoderm specification within regions of the EB close to the *Cdh3*-*Wnt3a*-expressing HEK source, resulting in pattern elaboration and symmetry breaking within EBs. This synthetic biology-based approach puts us closer towards engineering synthetic organizers to improve the realism in stem cell-derived structures.

Keywords: Self-organization, Patterning, Symmetry breaking, Synthetic Biology, Wnt3a, Embryoid Body

Introduction

Self-organization is a central theme in developmental biology and regenerative medicine. It describes the inherent property of a multicellular system to acquire order through interactions among its constituent parts.[1] One facet of self-organization is pattern formation, whereby different cell states constituting a multicellular system arrange themselves in non-random spatial distributions. Pattern formation can be coupled to growth, which expands the spatial field of the multicellular system.[2] Following growth, arrangements set by initial pattern formation events may be used to organize the emergence of further, finer patterns in a process termed pattern elaboration.[3] Patterning of tissues and organs often exhibits some form of large-scale asymmetry that is important for physiological function (e.g. kidney ureter, lung primary bronchus, eye optic nerve).[3,4] While biological research has focused on understanding how self-organization emerges during development, efforts in bioengineering systems to control patterning for purposes of tissue engineering have been limited.

Mechanisms of patterning have been traditionally studied in embryo development, through which an amorphous mass of cells yields a complex organism with defined anatomy and order. Classical embryology has shown that diffusible biochemical signalling ligands emanating from highly localized cell groups, termed organizers, play major roles in patterning embryonic systems.[5] Polarized sources of signal production, gradient-like signal diffusion, and level-dependent differential signal responses, constitute a paradigm for developmental patterning and organizing the induction/evocation of cell fates.[2,6,7] During mouse embryonic development (gastrulation stage), the basic body plan and archetypal lineages emerge through reciprocal interactions between the extraembryonic ectoderm, the embryo-yielding epiblast, and the transient primitive endoderm. The anterior visceral endoderm acts as an organizer by producing long-range inhibitors of the Wnt/β-catenin and Nodal/TGFβ pathways,[8–10] whereas the prospective embryo posterior is marked by expression of Wnt3, BMP4 and Nodal.[11–15] This arrangement polarizes Wnt, BMP, and Nodal signalling activities, patterning the embryo's anteroposterior axis and elaborating its organization.[16] When the pre-gastrulation pluripotent epiblast is extracted, cultured as embryonic stem cells (ESCs), and differentiated as three-dimensional embryoid bodies (EBs), elements of self-organization observed during *in vivo* gastrulation are only partially recapitulated *in vitro*. For example, while Wnt/β-catenin activation and mesoderm induction appear as polarized domains within EBs, they cover broad and diffuse areas.[17] This basic self-organization can be refined by converting EBs to gastruloids through the timely activation of the Wnt/β-catenin pathway.[18,19] Although emerging Wnt/β-catenin signalling activity and lineage domains are more compact, and situated within an elongating EB protrusion, this improvement occurs via EB-autonomous self-organization that is accompanied by delayed differentiation and the absence of anterior embryonic structures.[19,20] These limitations reflect the general inability of stem cell-derived structures to autonomously recapitulate high-scale order, perhaps due to absence of overarching organizers, and thus calls for the creation of tools to exogenously control stem cell patterning.

Bioengineering offers a bottom-up avenue to program stem cell organization. Colony micropatterning allows biophysical control over ESC differentiations, with archetypal embryonic lineages emerging as radial patterns[21,22] whose symmetry can be broken through polarized delivery of ligands via microfluidics.[23] Synthetic biology-based drug-inducible overexpression of transcription factors during ESC differentiation can also drive spontaneous pattern formation and self-organization, making possible the generation of tissue-like systems, organoids and embryo-like structures.[24–26] While innovative, these approaches require significant engineering of either ESCs[24–26] or their physical environment,[21–23] most are based on adherent two-dimensional cultures,[21–24] and none capture user-defined control over *bona fide* intercellular interactions (*i.e.* controlling signal emission from producer cells or recognition and response from recipient cells, while achieving *in situ* concurrence of producers and recipients). One attempt towards this direction uses HEK-293 cells constitutively expressing *Wnt3a* or *Dkk1* to skew the position of *T-brachyury* induction (which marks the nascent mesoderm) in EBs. This method suffers from requiring recurrent generation of transiently transfected cells, manual injection into hanging drops containing EBs, and lack of automatic organization between HEK-293 cells and EBs.[27] A synthetic biology method that is arguably most reminiscent of organizers uses human induced pluripotent stem cells (iPSCs) engineered to produce Sonic Hedgehog (SHH), a diffusible signalling protein that plays multiple roles during embryogenesis including brain development. When transgenic iPSCs were overlaid with wild-type iPSCs, and differentiated as chimeric cerebral organoids, localized SHH producers induced a long-range signalling response that specified posterior-ventral forebrain markers near the SHH source and anterior-dorsal markers distally, thus patterning cerebral organoids while breaking symmetry.[28] However, none of these approaches employs genetic programming to achieve autonomous pattern formation between signal-producing cells and the differentiating EB or organoid, requiring that signal-producing cells are manually coupled to EBs or organoids to achieve desired responses. This limitation hinders such cell-based methods in terms of efficiency,[28] automation,[27] and biological sophistication, reflecting the need for new and better systems.

We set out to provide a novel synthetic biology proof-of-concept application: naïve culture cells can be bioengineered to act as synthetic organizer-like systems, by programming them to undergo pattern formation with EBs, impose localized and polarized signalling events, and drive a controlled differentiation arrangement/outcome. Using HEK-293 cells as the chassis, we have established self-organizing signalling centres that control EB pattern elaboration (Figure 1). Pattern formation is achieved via differential adhesion, whereby HEK cells synthetically expressing P-cadherin (*Cdh3*) automatically segregate from ESCs naturally expressing E-cadherin (*Cdh1*), leading to self-organizing HEK aggregates decorating the exterior of EBs. If these adjoining aggregates also express *Wnt3a*, EBs respond with a polarized β-catenin activity gradient, with most *T-brachyury*-marked nascent mesoderm emerging proximal to synthetic signalling centres. This proof-of-concept demonstrates our ability to bioengineer synthetic cell systems that combine *i) de novo* pattern formation *ii)* with subsequent pattern

elaboration based on *bona fide* cell-cell interactions *iii)* when applied to stem cell-derived structures, providing the foundation for potential future applications.

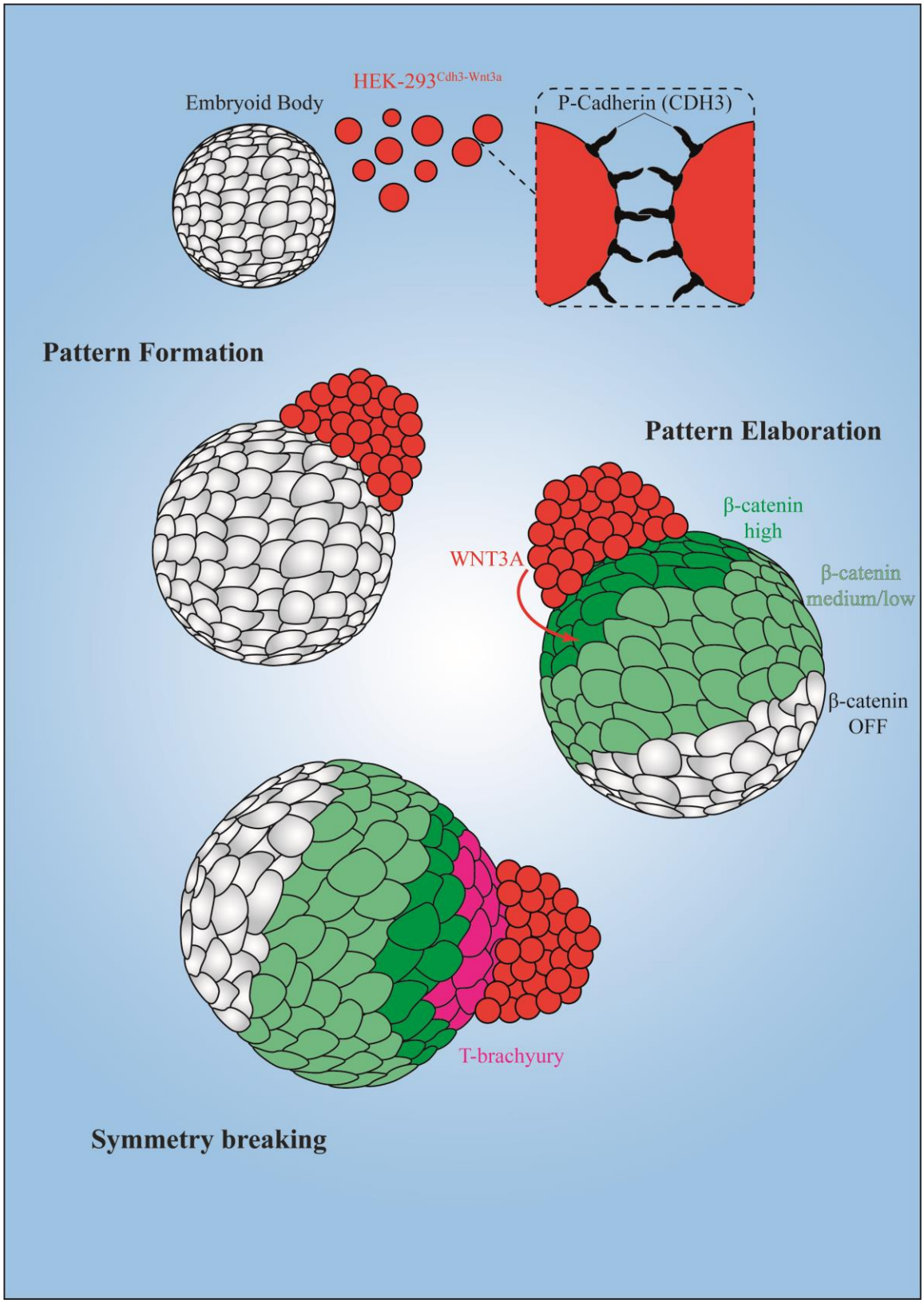

Figure 1. Graphical overview of synthetic biology cell-based system to control stem cell self-organization. Mouse ESCs naturally expressing *Cdh1* form phase-separation patterns when co-cultured with HEK-293 cells synthetically expressing *Cdh3*. By adding *Wnt3a* expression to HEK-293 cells, EBs produce a polarized and gradient-like β-catenin activation response with respect to HEK-293 localization. Nascent mesoderm (T-brachyury+) is inducted predominantly juxtaposing HEK$^{Cdh3\text{-}Wnt3a}$.

Results and Discussion

Synthetic pattern formation between HEK^{Cdh3} and mESCs

The differential adhesion hypothesis postulates that, when two cell populations differ in homotypic adhesiveness, differential surface tensions drive segregation between heterotypic cells.[29] Based on this principle, we have previously established a synthetic system in which two HEK-293 cell line derivatives (HEK^{Cdh1} and HEK^{Cdh3} for succinctness; both TREx-293-derived) express different cadherins (E-cadherin/*Cdh1* or P-cadherin/*Cdh3*) in a tetracycline-inducible manner. A random mixture of these cells self-organizes into patch-like phase-separation patterns.[30] To investigate whether phase-separation patterns can be formed between HEK^{Cdh3} cells (marked by mCherry) and other cells that naturally express *Cdh1,* such as mESCs,[31] we co-cultured mESCs with HEK^{Cdh3} under tetracycline supplementation (to induce *Cdh3* expression in HEK^{Cdh3}) in 2D and 3D conditions. Live cell arrangements were visualized via fluorescence microscopy after 48 hours.

In 48-hour 2D co-cultures, HEK^{Cdh3} cells formed an mCherry+ lawn periodically interrupted by circular, oval, or more random-shaped islands of compact mESC colonies (reporter negative cells evident in the bright-field channel). This topography could be reversed to produce an arrangement of HEK^{Cdh3} islands interspaced within an mESC lawn instead, by modulating the mESC:HEK^{Cdh3} seeding ratio (Figure 2A). Each cell type organized into homotypic patches with well-defined borders, and intermingling between heterotypic cells was not apparent. The topography of HEK^{Cdh3} and mESCs, its sensitivity to seeding cell ratio/stoichiometry, and the lack of heterotypic cell intermingling in these co-cultures, were all comparable to HEK-based phase-separation patterns (Figure 2A, compare to Figure 3B and ref[30]). For 3D co-cultures, we aggregated mESCs into EBs and added tetracycline-induced HEK^{Cdh3} at 24h of differentiation. Chimeric aggregates comprising mCherry- (mESCs) and mCherry+ (HEK^{Cdh3}) cells could be seen as early as differentiation day 2 and grew stably up until day 4 when the experiment was terminated (Figure 2B). HEK^{Cdh3} cells localized as aggregated masses around a central EB rather than thoroughly intermingling with EB cells (Figure 2B). This segregation between heterotypic cell types, which leads to a mixed co-aggregate comprising self-organized population phases, is broadly comparable to HEK-based synthetic 3D phase-separation patterns (reproduced in Figure 2C and described by ref[30]). These experiments indicate that HEK^{Cdh3} and mESCs undergo *de novo* pattern formation when co-cultured in 2D and 3D conditions.

The dish-rotator method used to generate 3D co-aggregates is efficient while requiring a simple modification in the original differentiation protocol, allowing us to examine large numbers of aggregates (Supplemental Figure 1A). Across 304 multicellular aggregates over 8 independent experiments, only 1 (0.3%) was a pure EB, 39 (12.8%) contained only HEK-type cells, while 264 (86.9%) contained EBs with HEK-type aggregates attached (Supplemental Figure 1B). From the 264 co-aggregates, 252 (82.9% of total) comprised a single EB that was most frequently decorated with one

(n=85/252) or two (n=88/252) HEK-type aggregates (Supplemental Figure 1C-D); more than two HEK-type aggregates per EB were far less frequent (Supplemental Figure 1D). The remaining 12 (4.0% of total) co-aggregates comprised a central plate of HEK-type cells attached simultaneously to two EBs, creating a three-aggregate structure (see later sections). Altogether, this synthetic biology-based platform allows for the efficient and automatic formation of patterned co-cultures comprising HEK^{Cdh3}-based cells and mESCs in phase-separation, in both 2D and 3D conditions.

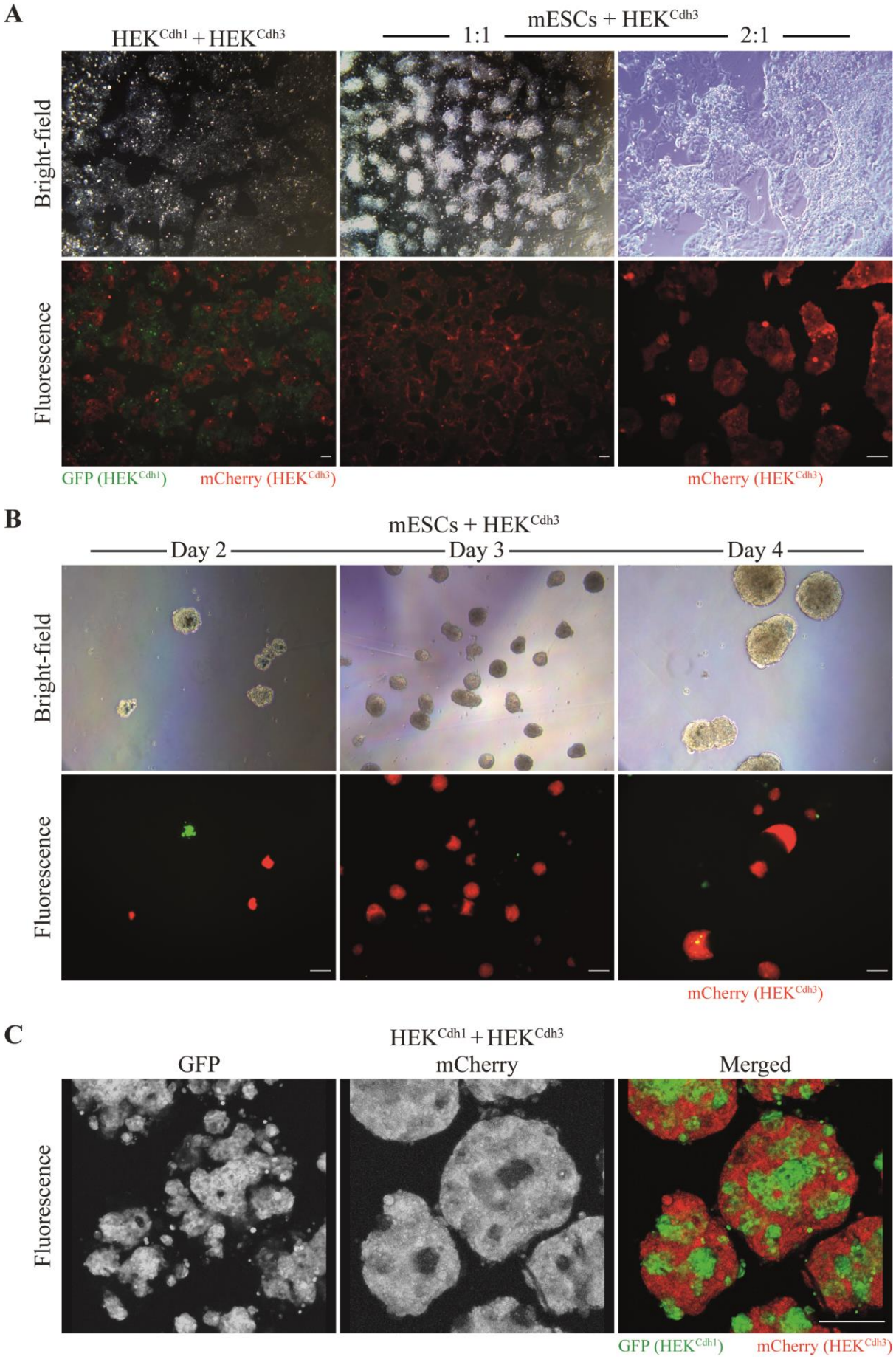
A
HEK^Cdh1 + HEK^Cdh3
mESCs + HEK^Cdh3
1:1
2:1
Bright-field
Fluorescence
GFP (HEK^Cdh1)
mCherry (HEK^Cdh3)
mCherry (HEK^Cdh3)
B
mESCs + HEK^Cdh3
Day 2
Day 3
Day 4
Bright-field
Fluorescence
mCherry (HEK^Cdh3)
C
HEK^Cdh1 + HEK^Cdh3
GFP
mCherry
Merged
Fluorescence
GFP (HEK^Cdh1)
mCherry (HEK^Cdh3)

Figure 2. ESCs and HEK^{Cdh3} self-organize into phase-separation patterns. (A) Fluorescence microscopy of live tetracycline-supplemented 48h adherent co-cultures between mESCs and HEK^{Cdh3}, mixed in a 1:1 or 2:1 ratio. A positive control phase-separation pattern co-culture (HEK^{Cdh1}+HEK^{Cdh3}) is also provided. Scale bars: 200μm. **(B)** Fluorescence microscopy of live EBs differentiated with the addition of HEK^{Cdh3} at 24h after EB formation. Green signal is cell death-related autofluorescence. Images were taken at 48h, 72h and 96h of differentiation. Scale bars: 200μm. **(C)** Confocal microscopy covering a short depth from the surface of live phase-separation co-aggregates, formed between HEK^{Cdh1} and HEK^{Cdh3} (≈1:2 ratio), and serving as a positive pattern control. Scale bar: 200μm. Experiments and results in (A-B) were replicated at least four times.

WNT3A production from self-organizing HEK^{Cdh3} cells

Phase-separation patterning between HEK^{Cdh3} and mESCs offers a unique opportunity to evoke organized signalling events, whereby signals emanating from self-organizing HEK^{Cdh3} aggregates act locally on mESC-derived EBs during co-culture. This can be realized by further engineering HEK^{Cdh3} to produce and secrete a signalling ligand that possesses limited diffusion (thus being retained close to source cells), but does not abrogate the initial pattern formation mechanics. *Wnt3a* was chosen due to its efficient secretion,[32] limited diffusion,[33] ability to promote primitive streak induction during gastrulation and EB differentiation,[17,34] and prevalent roles in developmental and stem cell fate decisions in various contexts.[32–37] We introduced constitutive expression of murine *Wnt3a* to HEK^{Cdh3} cells through random integration of a *CMV::mCherry-2A-Wnt3a* module (Figure 3A). To validate that the modified HEK^{Cdh3} derivatives (HEK$^{Cdh3\text{-}Wnt3a}$) retained pattern formation capacity, HEK$^{Cdh3\text{-}Wnt3a}$ or parental controls were co-cultured with HEK^{Cdh1} under tetracycline supplementation to elicit phase-separation. In 2D co-cultures, HEK$^{Cdh3\text{-}Wnt3a}$ formed characteristic phase-separation patterns with HEK^{Cdh1}, akin to HEK^{Cdh3}/HEK^{Cdh1} controls (Figure 3B). Partial or complete phase-separation between HEK$^{Cdh3\text{-}Wnt3a}$ and HEK^{Cdh1} was also observed in 3D co-cultures depending on the number of cells seeded (Figure 3C), as previously shown for HEK^{Cdh3}/HEK^{Cdh1} phase-separation.[30] Hence, addition of the *Wnt3a* expression module to HEK^{Cdh3} did not interfere with adhesion-driven pattern formation mechanics.

To assess WNT3A production and secretion by HEK$^{Cdh3\text{-}Wnt3a}$, and whether WNT3A can activate the Wnt/β-catenin pathway in receiver cells, a conditioned-medium approach was employed. Transgenic mESCs that report for Wnt/β-catenin pathway activation via GFP fluorescence have been described previously.[17] These mESCs produced quantifiable fluorescence when stimulated with CHIRON-99021 (a GSK3B antagonist, and thus Wnt/β-catenin pathway agonist), or human recombinant WNT3A, for 24h (Figure 4A-B). Culture media conditioned by HEK$^{Cdh3\text{-}Wnt3a}$, but not by HEK^{Cdh3}, visibly activated GFP fluorescence when supplied to reporter mESCs for 24h (Figure 4C). Relative to maintenance medium, HEK^{Cdh3}-conditioned media showed no convincing capacity in increasing the fold-change of quantifiable GFP fluorescence (mean (μ)=1.7, SEM=0.7, n=3 independent experiments), whereas HEK$^{Cdh3\text{-}Wnt3a}$-conditioned media produced a clear effect (μ=10.7, SEM=1.7, n=3 independent experiments) (Figure 4D). When fluorescence values across three independent experiments were pooled, measurements from HEK^{Cdh3}-conditioned samples were not significantly different from maintenance controls (P=0.9985, n=31 colonies), whereas fluorescence from HEK$^{Cdh3\text{-}Wnt3a}$-conditioned samples was significantly higher compared to HEK^{Cdh3} (P=0.0008, n=31 colonies, one-way ANOVA with Tukey's multiple comparisons). This was consistent across experiments (Supplemental Figure 2). Together, these results show the successful modification of the phase-separation patterning system to secrete biologically functional WNT3A from HEK^{Cdh3}, without compromising the cells' ability to undergo *de novo* pattern formation when co-cultured with HEK^{Cdh1}.

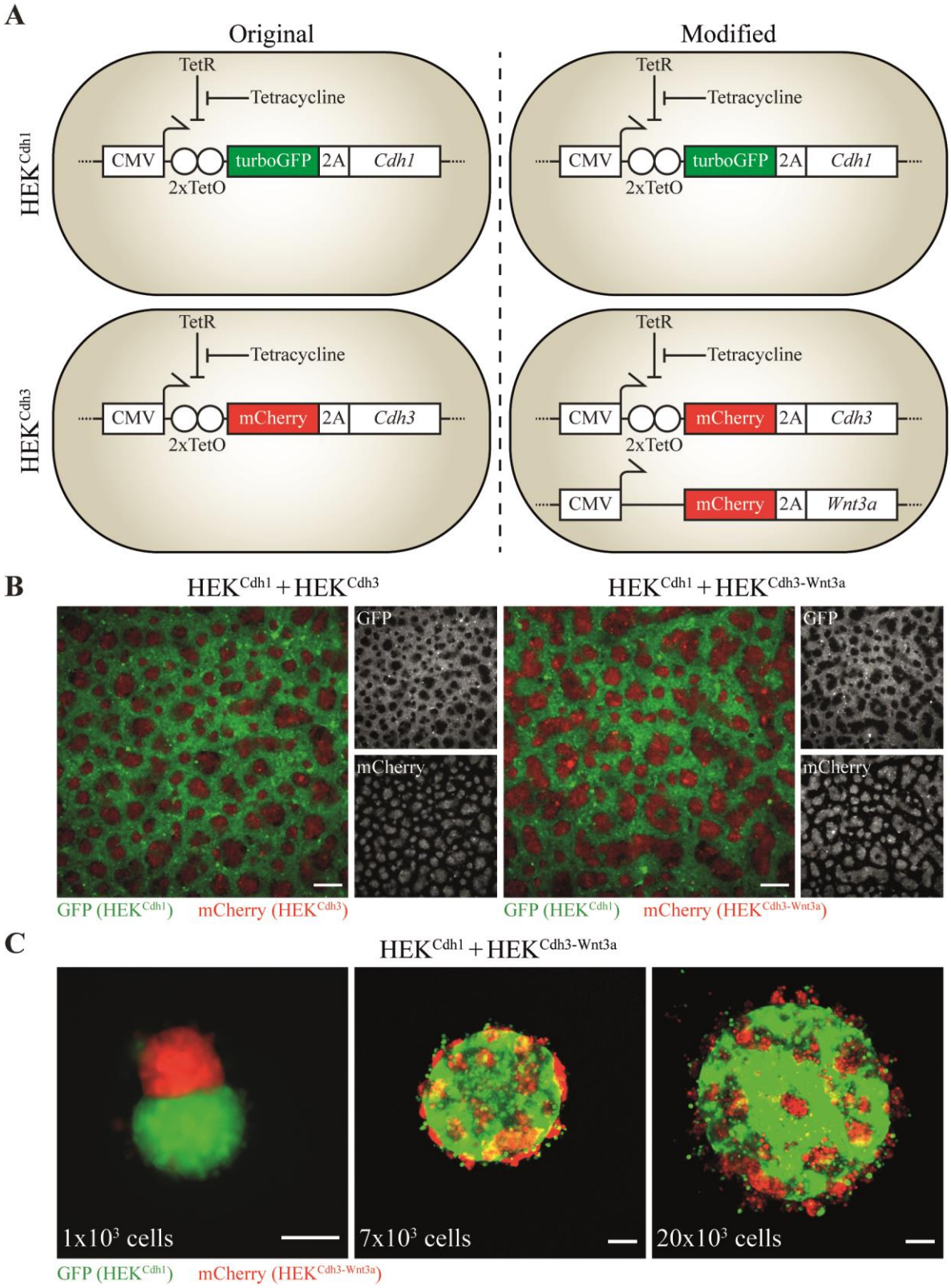

Figure 3. Modified HEK^{Cdh3} derivatives (HEK$^{Cdh3\text{-}Wnt3a}$) retain pattern formation capacity. (A) Schematic overview of synthetic biology cell systems. Left: HEK-293 cells stably expressing TetR (TREx-293) previously engineered to overexpress *turboGFP* and *Cdh1* (HEK^{Cdh1}) or *mCherry* and *Cdh3* (HEK^{Cdh3}) in a tetracycline-inducible manner. Right: HEK^{Cdh3} was modified to constitutively

express *mCherry* and *Wnt3a* via random integration of *CMV::mCherry-2A-Wnt3a* transgene. **(B)** Phase-separation patterning between HEK^{Cdh1} and HEK^{Cdh3}-based cells in live 24h adherent cultures. Left: co-cultures using the original HEK^{Cdh1}/HEK^{Cdh3} system. Right: co-cultures using the modified HEK^{Cdh1}/$HEK^{Cdh3\text{-}Wnt3a}$ system. Large panels show overlay of green and red channel fluorescence. Small panels show single channels in grayscale (top: green; bottom: red) Scale bars: 200μm. **(C)** Complete or partial three-dimensional phase-separation patterning between modified $HEK^{Cdh3\text{-}Wnt3a}$ and HEK^{Cdh1}, depending on total cells seeded. Live samples were imaged after 24h of co-culture. Scale bars: 100μm.

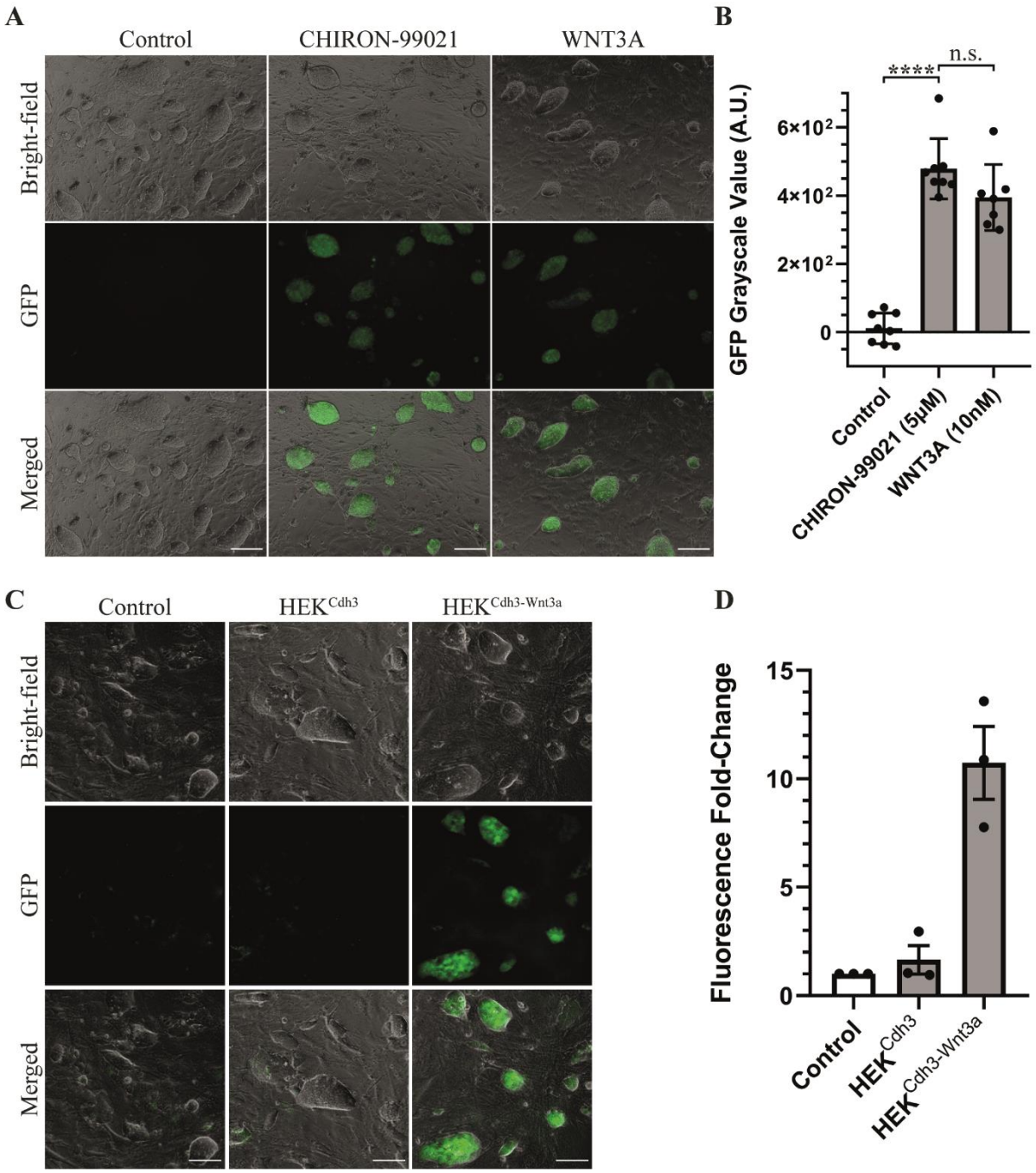

Figure 4. HEK$^{Cdh3\text{-}Wnt3a}$ produce and secrete biologically functional WNT3A in the culture medium. (A) Fluorescence microscopy of live Wnt/β-catenin *7xTCF/LEF::eGFP* mESC reporters[17] cultured for 24h using control maintenance medium, or additionally containing CHIRON-99021 (5μM) or human recombinant WNT3A (10nM). Scale bars: 100μm. **(B)** Quantification of colony fluorescence from panels shown in (A). From each colony, the average image background was subtracted. Columns show means, error bars show standard deviations. Statistic: One-way ANOVA with Tukey's multiple comparisons. ****, P<0.0001. **(C)** Fluorescence microscopy of live Wnt/β-catenin *7xTCF/LEF::eGFP* mESC reporters cultured for 24h using control maintenance medium, or maintenance medium diluted 50% with medium conditioned by HEK^{Cdh3} or HEK$^{Cdh3\text{-}Wnt3a}$. Scale bars: 100μm. **(D)** Quantification of

mean GFP fluorescence intensity from three experiments as in (C). Each datum point represents an experimental mean fluorescence intensity, expressed relative to its paired maintenance medium control, for three independent experiments. Columns shows means of pair-wise normalized means and error bars standard error of the mean. For individual experiments, see Supplemental Figure 2.

Gradient-like signalling between HEK$^{Cdh3\text{-}Wnt3a}$ and EBs

To investigate whether the combination of pattern formation and signalling from HEK$^{Cdh3\text{-}Wnt3a}$ can elicit localized events in mESCs, we co-cultured Wnt/β-catenin reporter mESCs (*7xTCF/LEF::eGFP*) with *Cdh3* and *Wnt3a*-expressing HEK$^{Cdh3\text{-}Wnt3a}$ cells. In live adherent cultures, mESCs formed phase-separation patterns with HEK$^{Cdh3\text{-}Wnt3a}$ cells (Figure 5A), similar to aforementioned mESC/HEK^{Cdh3} co-cultures (Figure 2A). ESC colonies from HEK$^{Cdh3\text{-}Wnt3a}$, but not HEK^{Cdh3} co-cultures, emitted green fluorescence marking Wnt/β-catenin activation due to HEK$^{Cdh3\text{-}Wnt3a}$-derived WNT3A (Figure 5A). This dual control over patterning and signalling is even more clear in fixed immunostained samples (Figure 5B). These observations corroborate the stability of HEK$^{Cdh3\text{-}Wnt3a}$ in initiating pattern formation and signalling events when co-cultured with mESCs.

In 3D conditions, Wnt/β-catenin reporter EBs were grown in co-culture with HEK$^{Cdh3\text{-}Wnt3a}$, HEK^{Cdh3}, or standalone. Differentiations were carried out until day 4, which is the peak of *T-brachyury* induction that marks the primitive streak and nascent mesoderm.[17,38] On day 3, green fluorescence was apparent in the EB portion of EB-HEK$^{Cdh3\text{-}Wnt3a}$ co-aggregates, whereas standalone or HEK^{Cdh3}-supplied cultures produced no visible GFP fluorescence (Figure 5C). This reflects exogenous activation of the Wnt/β-catenin pathway by means of HEK$^{Cdh3\text{-}Wnt3a}$ signalling, prior to endogenous activation through the intrinsic differentiation course which occurs between day 3.5 and day 4.[17] On day 4, Wnt/β-catenin pathway activation was evident across all conditions: in standalone differentiations, GFP fluorescence appeared diffuse and spread over large EB portions (Figure 5C) as previously reported.[17] Fluorescence appeared dimmer in EB-HEK^{Cdh3} co-aggregates and did not seem to arrange in any specific manner with regards to HEK^{Cdh3} positions (Figure 5C). The reasons behind the apparent attenuation of the Wnt/β-catenin pathway in EBs co-cultured with HEK^{Cdh3} cells are currently unknown, and this attenuation did not appear to disrupt the timing of *T-brachyury* induction (see following sections). EB-HEK$^{Cdh3\text{-}Wnt3a}$ co-aggregates demonstrated intense and polarized GFP signal: fluorescence was strongly evident in EB areas juxtaposed to HEK$^{Cdh3\text{-}Wnt3a}$ cells and gradually declined with increasing distance (Figure 5C). This polarization in β-catenin activation was most clearly seen in EBs carrying one small HEK$^{Cdh3\text{-}Wnt3a}$ aggregate, and on day 4 of differentiation. These results were reproducible over 4 independent experiments. We observed that, when mESCs and HEK$^{Cdh3\text{-}Wnt3a}$ were mixed on day 0, pattern formation and signalling still occurred but activation of the β-catenin GFP reporter was homogeneous rather than gradient-like, which defeats the purpose of our engineering approach.

Fluorescence quantification over distance shows that GFP formed a gradient extending over roughly 80-120μm (μ=98.9μm, SD=12.6μm, n=8 co-aggregates), peaking next to HEK$^{Cdh3\text{-}Wnt3a}$ aggregates and decreasing thereafter. Measurements were comparable whether they derived from GFP quantification of live samples using epifluorescence microscopy (n=4), or DAPI-normalized GFP quantification of fixed-immunostained samples using confocal laser scanning microscopy (n=4; Figure

6). The diminishing stage can be reliably modelled (R^2>0.95) using a one phase decay curve fit (Figure 6), which reveals that the GFP signal reaches its half-intensity around 30μm (μ=31.7μm, SD=6.7μm, n=8 co-aggregates) after the pre-decay maximum. Assuming an EB cell possesses a diameter between 5-10μm, it is suggested that the Wnt/β-catenin-reporting GFP signal loses 50% of its activity 3-5 EB cell layers past the $HEK^{Cdh3\text{-}Wnt3a}$ aggregate. These results were derived from EB-$HEK^{Cdh3\text{-}Wnt3a}$ co-aggregates in which $HEK^{Cdh3\text{-}Wnt3a}$ cells arranged in a highly localized manner, as opposed to morphologies in which the $HEK^{Cdh3\text{-}Wnt3a}$ aggregate curved around and overlaid a big fraction of the EB. Based on qualitative observations, the spread of Wnt/β-catenin activation depended on the geometrical composition of EB-$HEK^{Cdh3\text{-}Wnt3a}$ co-aggregates, rather than the size of the $HEK^{Cdh3\text{-}Wnt3a}$ signalling centre; deep investigation of this complex developmental topic is beyond the scope of this article. Altogether, these results demonstrate that synthetic $HEK^{Cdh3\text{-}Wnt3a}$ cells simultaneously apply phase-separation patterning and signalling when co-cultured with mESCs (2D) or EBs (3D), producing a $HEK^{Cdh3\text{-}Wnt3a}$ aggregate that evokes gradient-like activation of the Wnt/β-catenin pathway in EBs.

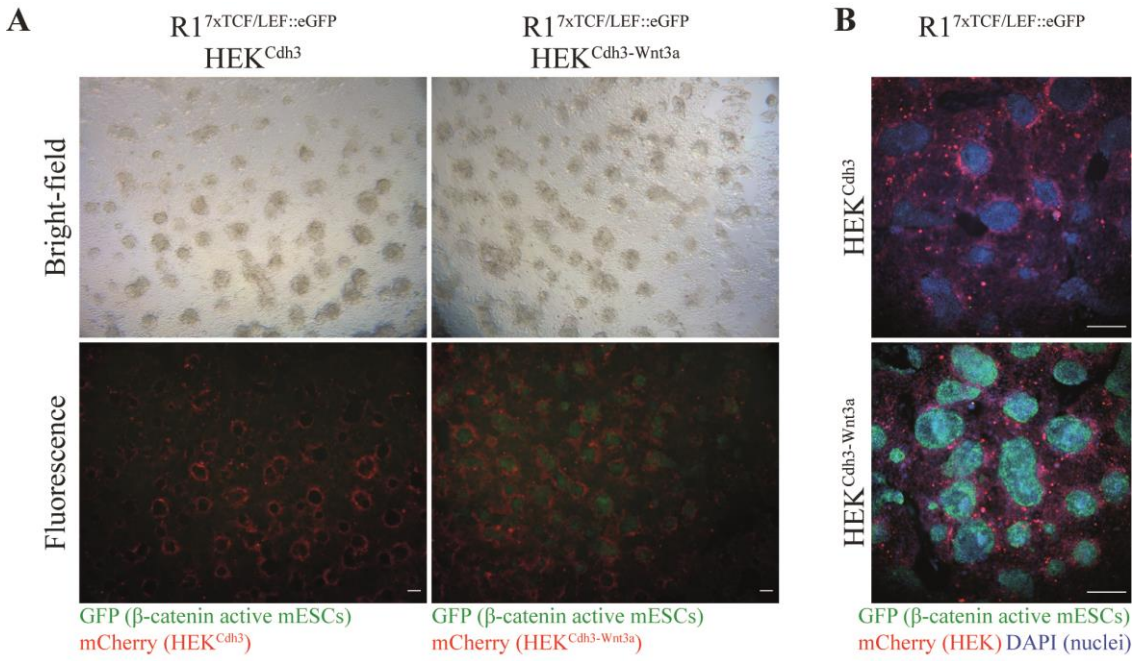
A
R1 7xTCF/LEF::eGFP
HEK Cdh3
R1 7xTCF/LEF::eGFP
HEK Cdh3-Wnt3a
Bright-field
Fluorescence
GFP (β-catenin active mESCs)
mCherry (HEK Cdh3)
GFP (β-catenin active mESCs)
mCherry (HEK Cdh3-Wnt3a)
B
R1 7xTCF/LEF::eGFP
HEK Cdh3
HEK Cdh3-Wnt3a
GFP (β-catenin active mESCs)
mCherry (HEK) DAPI (nuclei)

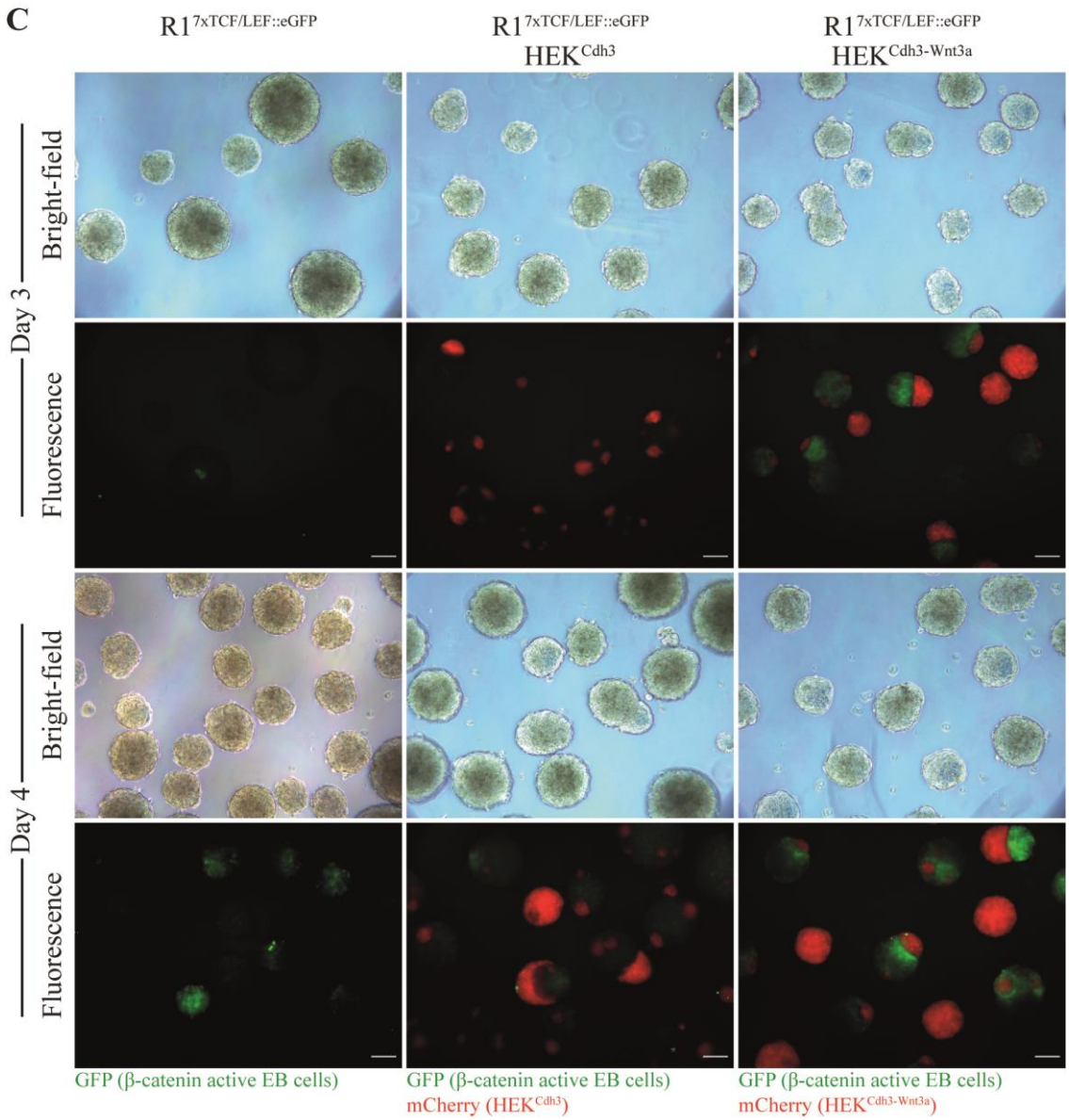
C
R1 7xTCF/LEF::eGFP
R1 7xTCF/LEF::eGFP
HEK Cdh3
R1 7xTCF/LEF::eGFP
HEK Cdh3-Wnt3a
Day 3
Bright-field
Fluorescence
Day 4
Bright-field
Fluorescence
GFP (β-catenin active EB cells)
GFP (β-catenin active EB cells)
mCherry (HEK Cdh3)
GFP (β-catenin active EB cells)
mCherry (HEK Cdh3-Wnt3a)

Figure 5. HEK$^{Cdh3\text{-}Wnt3a}$ activate the Wnt/β-catenin pathway in mESCs in phase-separation, and elicit gradient-like responses in EBs. (A) Fluorescence microscopy of live tetracycline-supplemented 48h adherent co-cultures between *7xTCF/LEF::eGFP* mESCs and HEK^{Cdh3} or HEK$^{Cdh3\text{-}Wnt3a}$. Scale bars: 200μm. **(B)** Fluorescence microscopy of fixed and immunostained 96h adherent co-cultures between *7xTCF/LEF::eGFP* mESCs and HEK^{Cdh3} or HEK$^{Cdh3\text{-}Wnt3a}$, counterstained with DAPI. Scale bars: 200μm. **(C)** Fluorescence microscopy of *7xTCF/LEF::eGFP* EBs differentiated standalone, with the addition of HEK^{Cdh3}, or the addition of HEK$^{Cdh3\text{-}Wnt3a}$ at 24h after EB formation. Images were taken at 72h or 96h of differentiation. Scale bars: 200μm. Experiments and results were replicated four times.

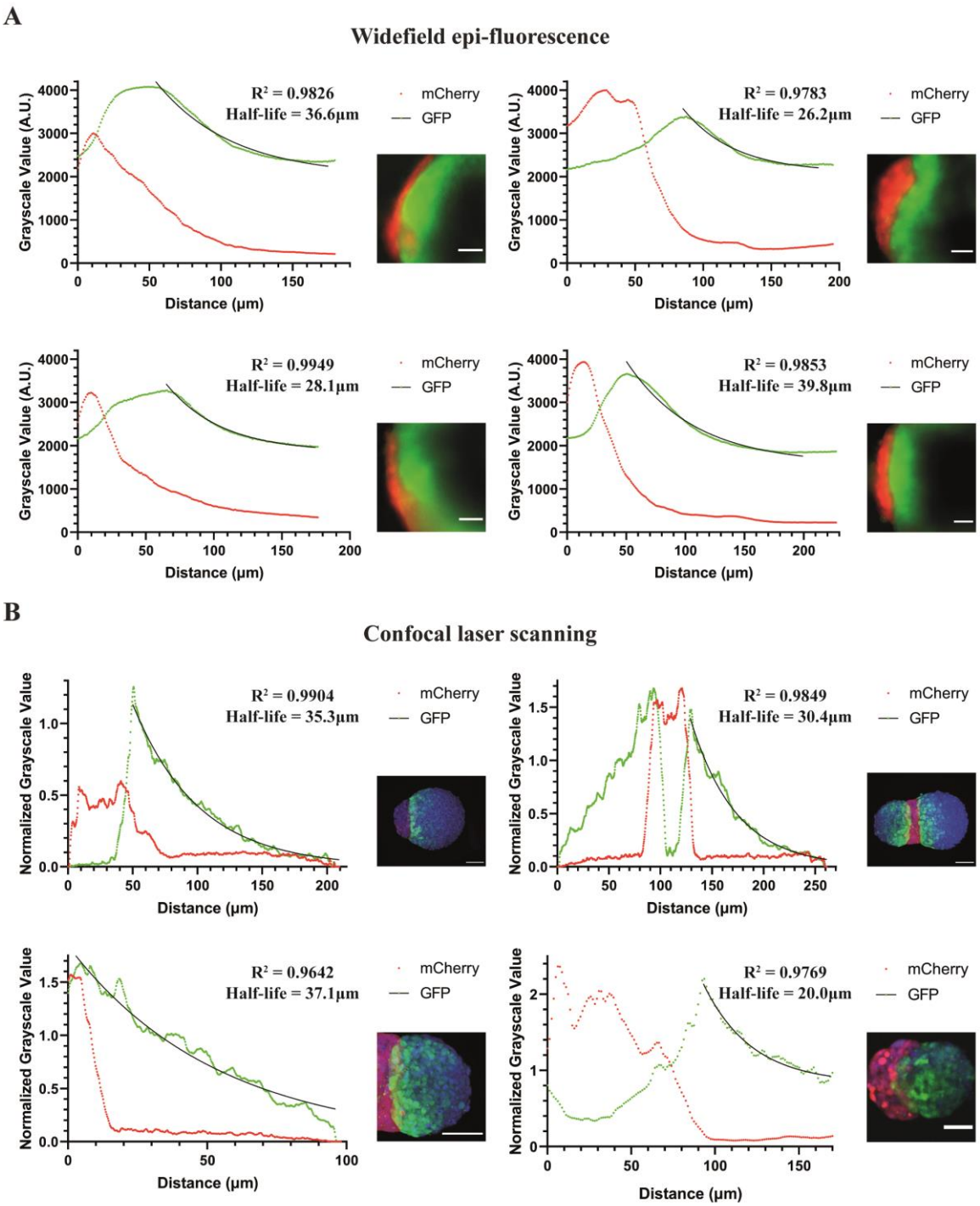

Figure 6. Quantification of Wnt/β-catenin activation gradient in EB-HEK$^{Cdh3\text{-}Wnt3a}$ co-aggregates. **(A)** Fluorescence quantification of 4 independently cultured co-aggregates comprising *7xTCF/LEF::eGFP* mESCs and HEK$^{Cdh3\text{-}Wnt3a}$ cells, live-imaged at day 4 using a widefield epi-fluorescence inverted microscope. Red dots (mCherry) show the HEK$^{Cdh3\text{-}Wnt3a}$ aggregate position, green dots (GFP) show the area of Wnt/β-catenin activation, and black lines represent best fit curves over the distance of decreasing GFP fluorescence intensity using a one phase decay model. Scale bars: 50µm. **(B)** Quantifications as in (A) based on fixed and immunostained samples imaged via confocal laser scanning microscopy. Values in (B) are normalized to DAPI. Scale bars: 50µm.

HEK$^{Cdh3\text{-}Wnt3a}$ cells control localization of T-brachyury induction

To better interrogate the effect of HEK$^{Cdh3\text{-}Wnt3a}$ in the localization of Wnt/β-catenin pathway activation and nascent mesoderm induction, EB-HEK$^{Cdh3\text{-}Wnt3a}$ co-aggregates were fixed and stained for mCherry (HEK$^{Cdh3\text{-}Wnt3a}$), GFP (β-catenin-active cells) and T-brachyury (nascent mesoderm). Confocal imaging confirmed the polarized and gradual activation of the Wnt/β-catenin pathway with respect to HEK$^{Cdh3\text{-}Wnt3a}$ localization, as GFP appeared intense close to mCherry signal and decreased with increasing distance (Figure 7A, Figure 6B). In addition, the majority of T-brachyury+ cells (magenta) within the EB localized nearby mCherry+ HEK$^{Cdh3\text{-}Wnt3a}$ cells (Figure 7A). In rare cases where two EBs were cross-linked via one HEK$^{Cdh3\text{-}Wnt3a}$ aggregate belt, both EBs showed strong Wnt/β-catenin pathway activation (GFP) close to the common HEK$^{Cdh3\text{-}Wnt3a}$ 'organizer', the signal of which decreased over distance in oppositely-oriented gradients. In these structures, T-brachyury (magenta) stain was predominantly seen in EB areas juxtaposing the HEK$^{Cdh3\text{-}Wnt3a}$ belt (Figure 7B). However, we note that not all T-brachyury+ cells observed were exclusively located next to HEK$^{Cdh3\text{-}Wnt3a}$ aggregates (Figure 7A-B).

To confirm these findings on a larger scale, EB differentiations were repeated using *T-brachyury::eGFP* reporter mESCs established previously.[38] On day 4, standalone EB differentiations demonstrated endogenous GFP expression (*T-brachyury*), the signal of which adopted a diffuse distribution over large EB areas (Figure 7C). Control EB-HEK^{Cdh3} co-aggregates showed no clear localization of GFP with respect to mCherry (Figure 7C). In contrast, when EB-HEK co-aggregates were made using HEK$^{Cdh3\text{-}Wnt3a}$, the *T-brachyury*-reporting GFP signal was predominantly localized next to or near mCherry+ HEK$^{Cdh3\text{-}Wnt3a}$ cells (Figure 7C). Fluorescence intensity profiles confirm that HEK$^{Cdh3\text{-}Wnt3a}$ cells skewed the distribution of *T-brachyury* expression towards the HEK aggregate, whereas HEK^{Cdh3} cells appeared not to exert such effect (Figure 7D). No GFP was apparent in any condition on day 3 (not shown). These observations surrounding *T-brachyury::eGFP* expression patterns were reproducibly seen across 4 independent experiments, and largely reflect aforementioned *7xTCF/LEF::eGFP* differentiations with respect to localization (compare Figure 5C to Figure 7C). Overall, these results corroborate that in EB-HEK$^{Cdh3\text{-}Wnt3a}$ co-aggregates, the location of nascent mesoderm evocation is predominantly determined by the position of the HEK$^{Cdh3\text{-}Wnt3a}$ inducer body.

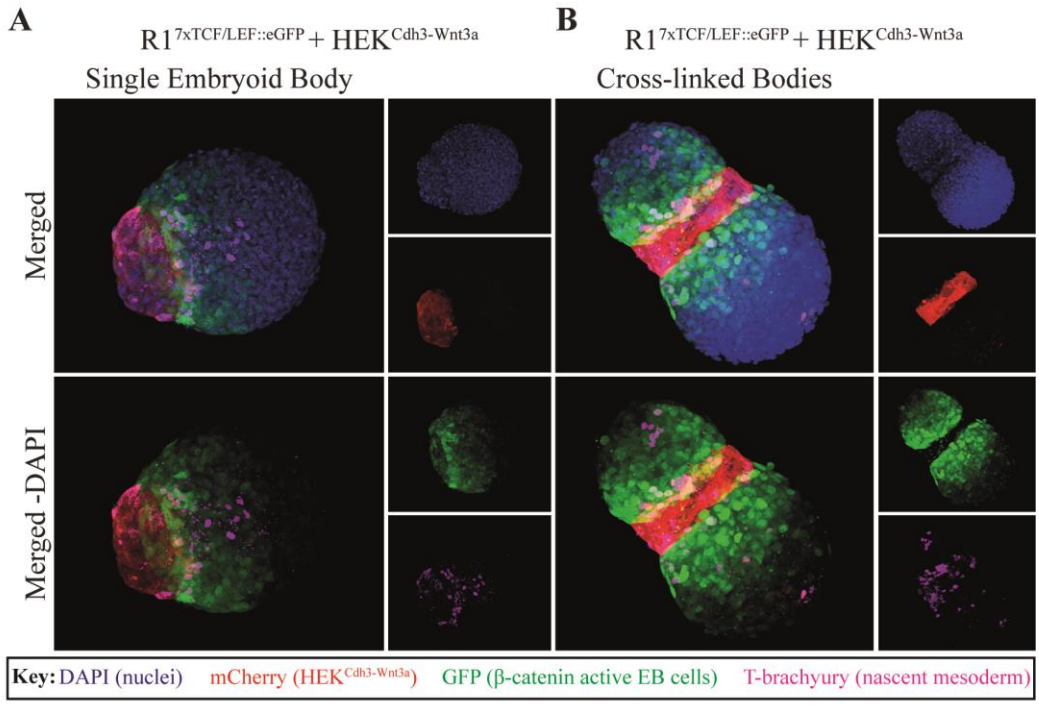
A
R1 7xTCF/LEF::eGFP + HEK Cdh3-Wnt3a
Single Embryoid Body
B
R1 7xTCF/LEF::eGFP + HEK Cdh3-Wnt3a
Cross-linked Bodies
Merged
Merged -DAPI
Key: DAPI (nuclei) mCherry (HEK Cdh3-Wnt3a) GFP (β-catenin active EB cells) T-brachyury (nascent mesoderm)

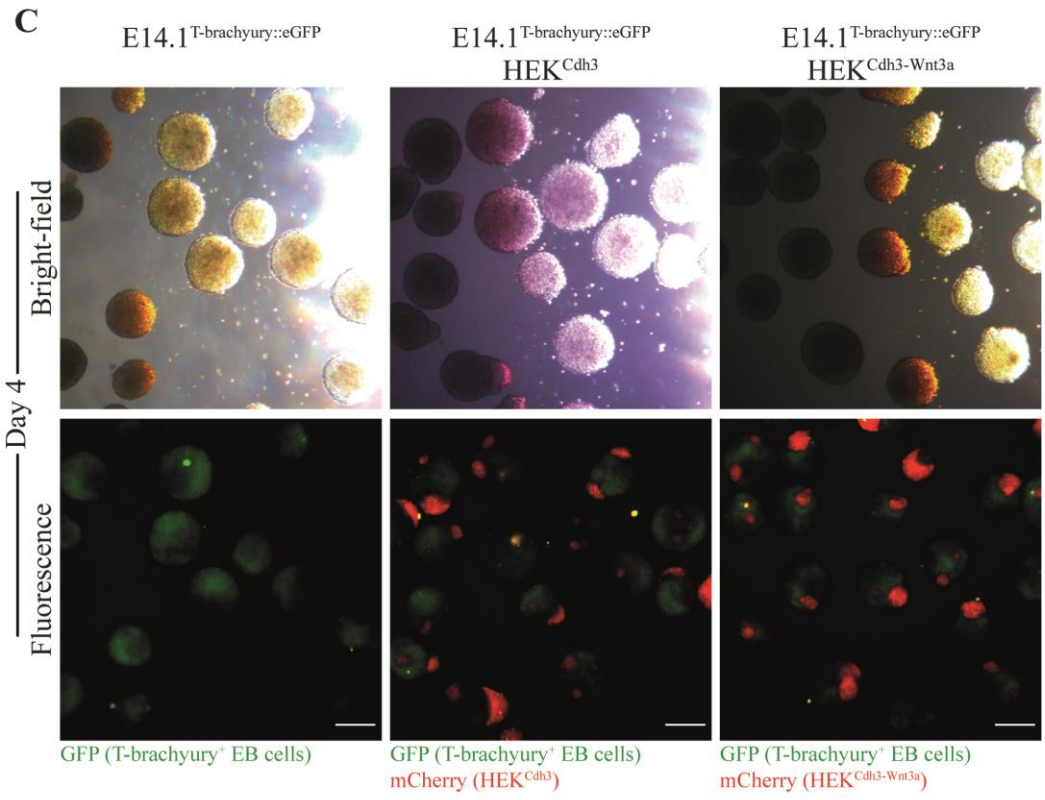
C
E14.1 T-brachyury::eGFP
E14.1 T-brachyury::eGFP
HEK Cdh3
E14.1 T-brachyury::eGFP
HEK Cdh3-Wnt3a
Day 4
Bright-field
Fluorescence
GFP (T-brachyury+ EB cells)
GFP (T-brachyury+ EB cells)
mCherry (HEK Cdh3)
GFP (T-brachyury+ EB cells)
mCherry (HEK Cdh3-Wnt3a)

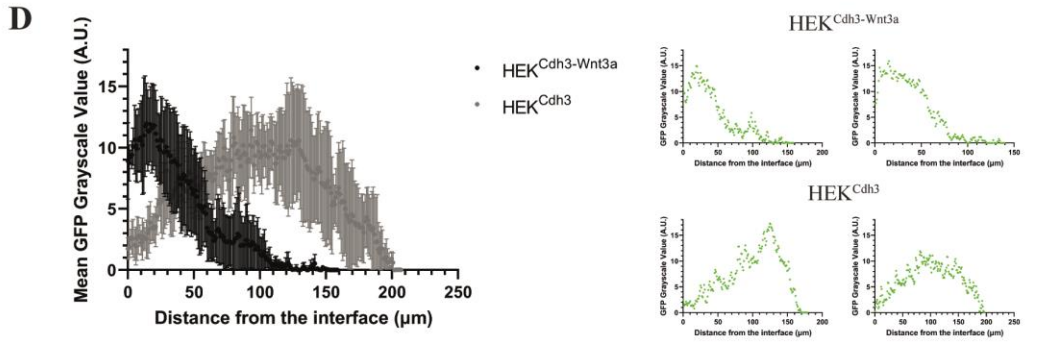
D
Mean GFP Grayscale Value (A.U.)
Distance from the interface (μm)
HEK Cdh3-Wnt3a
HEK Cdh3
HEK Cdh3-Wnt3a
HEK Cdh3

Figure 7. T-brachyury specification predominantly occurs at EB locales juxtaposing HEK$^{Cdh3\text{-}Wnt3a}$. (A-B) 3D-projections of whole-imaged, BABB-cleared EB-HEK co-aggregates, comprising a single *7xTCF/LEF::eGFP* EB carrying a single HEK$^{Cdh3\text{-}Wnt3a}$ aggregate **(A)**, or two *7xTCF/LEF::eGFP* EBs cross-linked by a single HEK$^{Cdh3\text{-}Wnt3a}$ aggregate belt **(B)**. For both (A-B), large panels show images of all colour-channels merged together (top large panels), or excluding DAPI (bottom large panels), and small panels show individual channels (blue: DAPI; red: mCherry reporting HEK$^{Cdh3\text{-}Wnt3a}$; green: eGFP reporting β-catenin-active EB cells; magenta: T-brachyury). Samples were imaged at x40 objective magnification, 1.15 zoom. **(C)** Fluorescence microscopy of live *T-brachyury::eGFP* EBs differentiated standalone, with the addition of HEK^{Cdh3}, or the addition of HEK$^{Cdh3\text{-}Wnt3a}$ at 24h after EB formation. Images were taken at 96h of differentiation. Experiments and results in (C) were replicated four times. Scale bars: 200μm. **(D)** *T-brachyury::GFP* fluorescence intensity plotted against increasing distance from the EB-HEK interface. Scatter dots/points show means, error bars show standard deviations of 5 co-aggregates as shown in (C). Small panels on the right are examples of individual measurements.

Self-organized WNT3A sources affect T-brachyury location, but not total expression

We wanted to address the quantitative effects of the EB-HEK phase-separation differentiation in the induction of prospective mesoderm. Day 4 EBs from *T-brachyury::eGFP* mESCs were dissociated and analyzed in terms of GFP-/GFP+ percentages via flow cytometry, following elimination of mCherry+ HEK^{Cdh3}/$HEK^{Cdh3\text{-}Wnt3a}$ cells. This gating strategy workflow (Supplemental Figure 3) allowed for distinction of GFP- and GFP+ mESC-derived populations from EB-HEK co-aggregates (Figure 8A). Differentiations exhibited considerable variation in terms of *T-brachyury::GFP* output over separate experiments despite controlling for medium and culture conditions, reflecting the widely-known inherent variation of ESC differentiation efficiencies. Control HEK^{Cdh3}-supplied differentiations consistently yielded reduced GFP percentages compared to standalone controls (Figure 8B-C, $P<0.05$, n=5 independent experiments, one-way ANOVA with Tukey's multiple comparisons). $HEK^{Cdh3\text{-}Wnt3a}$-supplied differentiations demonstrated less variance in GFP output (Figure 8B) and mixed effects: experiments in which standalone controls produced high GFP yield, $HEK^{Cdh3\text{-}Wnt3a}$-supplied samples showed reduced GFP output, whereas experiments with low GFP control yields showed increased output in $HEK^{Cdh3\text{-}Wnt3a}$-supplied samples (Figure 8C). To test whether $HEK^{Cdh3\text{-}Wnt3a}$ normalize T-brachyury yields in EBs, the variance of GFP+ percentages of $HEK^{Cdh3\text{-}Wnt3a}$-supplied samples was compared to that of standalone differentiations. Variances did not appear significantly different through an F-test ($P=0.16$) or a Kolmogorov-Smirnov test ($P=0.08$, n=5 independent experiments). Furthermore, GFP fluorescence intensity did not differ across conditions (Figure 8D-E). Hence, HEK^{Cdh3} reduce the T-brachyury+ fraction in EBs, whereas $HEK^{Cdh3\text{-}Wnt3a}$ produce no statistically clear quantitative effect in T-brachyury+ yield. Altogether, these findings demonstrate that $HEK^{Cdh3\text{-}Wnt3a}$ cells affect the location of T-brachyury induction, without affecting the amount of T-brachyury induced per differentiation.

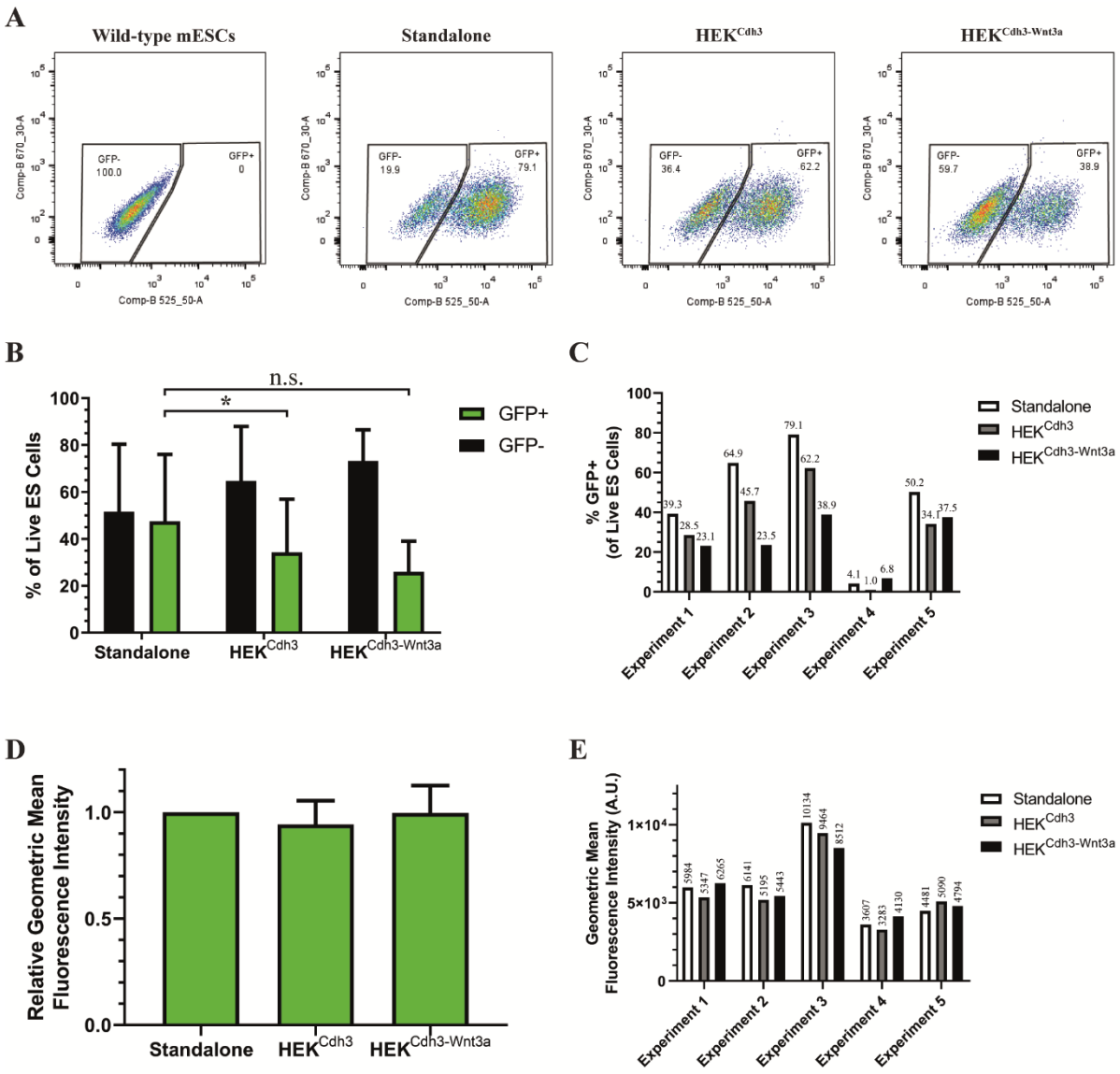

Figure 8. Flow cytometry analyses of *T-brachyury::eGFP* EBs at 96h of differentiation. (A) Example flow cytometry GFP analysis panels. From left to right: wild-type IB10 mESCs, *T-brachyury::eGFP* EBs differentiated standalone, *T-brachyury::eGFP* EBs differentiated under HEK^{Cdh3} phase-separation, and *T-brachyury::eGFP* EBs differentiated under HEK$^{Cdh3\text{-}Wnt3a}$ phase-separation. Panels are from the same experiment and show discrimination between GFP- and GFP+ events (525nm emission channel, X-axis), plotted against an auto-fluorescence far-red channel (670nm emission channel, Y-axis). For details on gating strategy, see Supplemental Figure 3. **(B)** Percentages of GFP- and GFP+ compartments for standalone, HEK^{Cdh3}-supplied, or HEK$^{Cdh3\text{-}Wnt3a}$-supplied differentiations of *T-brachyury::eGFP* EBs at 96h of differentiation. Columns show means, error bars show standard deviations for five independent experiments. Statistic: One-way ANOVA with Tukey's multiple comparisons. *, P<0.05. **(C)** Breakdown of GFP+ compartment percentages per individual experiment, from plots shown in (B). **(D)** Geometric mean fluorescence intensities of GFP+ compartments; results were expressed relative to control as different experiments were analyzed in

different cytometers. Columns show means, error bars show standard deviations from five independent experiments. **(E)** Breakdown of GFP geometric mean fluorescence intensities of GFP+ compartments per individual experiment, from plots shown in (D).

Discussion

In this study, we have proved the concept that the programming of pattern formation and signalling properties can be used to convert naïve cells into factor-elaborating devices that can control the localization of lineage specification during ESC differentiation. By exploiting our previously established synthetic patterning system,[29,30] pattern formation was achieved between HEK cells overexpressing P-cadherin and mESCs or mESC-derived EBs expressing E-cadherin. When these HEK cells were further modified to produce WNT3A, they elicited a gradient-like β-catenin activation response that resulted in *T-brachyury*-expressing cells at the HEK-specified EB pole (Figure 1).

Technological Advances

Developmental and stem cell research has been historically interested with understanding and controlling self-organization, which has led to the emergence of physical, biochemical and genetic technologies that target self-organization. This includes ESC micropatterning that facilitates the study of pattern formation as a result of emergent inductions,[21,22,39–41] and microfluidics that allow polarized provision of signalling agonists or antagonists to control pattern formation and symmetry breaking.[23] However, these methods rely on 2D adherent culture and biochemically purified ligands, which do not realistically reproduce the complex intercellular interactions typically occurring in 3D geometry. The norm for studying self-organization under 3D conditions *in vitro* has relied on stem cell-derived aggregates that partially recapitulate facets of self-organization autonomously, such as ESC-derived EBs that decode molecular signals into broadly polarized signalling activity and lineage domains.[17,27] These models are gradually being refined and replaced by more advanced versions, such as gastruloids or synthetic embryo structures reconstructed using multiple stem cell types.[18–20,26] Construction of many advanced stem cell-derived systems has been driven by synthetic overexpression of lineage-defining transcription factors, which mediates specification of desired lineages followed by emergent self-organization.[1,24–26] These systems lack overarching organizers, with the exception of a breakthrough in which synthetic embryo-like structures recapitulate formation of the anterior visceral endoderm, a key organizer during gastrulation.[26] However, transcriptomic analyses reveal critical differences between natural and synthetic embryo compartments, many of them lying in the expression of signalling-related genes.[26] Hence, the field is limited by a lack of approaches to control signalling events in stem cell-derived aggregates and in a highly localized manner. Achieving such control has the potential to improve the organizational realism of most aggregate systems, fine-tune signalling in the most advanced versions, and test hypotheses related to signalling organization during development and organogenesis. Our approach is a direct contribution to this call.

Previous attempts to exogenously control localized signalling in EBs have been limited. One attempt, similar to our efforts, has introduced *Wnt3a* expression into HEK-293 cells to try and bias the location of *T-brachyury* induction in adjunct EBs. This method relies on the recurrent generation of transiently transgenic populations and their manual coupling to EBs suspended in hanging drops, which is heavily labour-intensive, limited in scalability, and entails variation at multiple levels.[27] Our approach utilizes stable, high-purity lines that generate large numbers of EB-HEK co-aggregates efficiently and with limited user input, circumventing aforementioned limitations. In addition, our system offers automatic self-organization between EBs and HEK cells based on genetic programming, evocation of signalling gradients in recipient EBs, and the potential for streamlined testing of desirable signalling ligands based on the HEK^{Cdh3} chassis. Because it employs living cells, our approach is superior to bead technology[42] as it captures *bona fide* cell-cell interactions, real-time production of bioactive ligand, and the potential to program expression of multiple ligands, signalling dynamics or communication loops. Overall, our synthetic biology system narrows the gap between the degree of control over patterning that is possible during 2D ESC differentiation (which lacks realistic developmental complexity), and the complexity inherent to 3D ESC differentiation (which lacks sophisticated exogenous control), by programming automatic pattern formation and signalling in cells. This demonstration highlights the potential of synthetic biology for stem cell research applications.

Challenges

The challenge of bioengineering signalling centres is the attempt to program complex molecular events (patterning, signalling) into complex systems (cells) for an even more complex context (development). The desired cell chassis needs to be characterized to assess what patterning and signalling genes are natively expressed, and if introduced transgenes can fully function in the chassis. For example, we did not have to co-express *Wnt3a* with any processing and secretion factors for its biogenesis, but such consideration might be required depending on ligand and chassis. Patterning and signalling modules should function orthogonally with respect to each other and to cell physiology, and remain resistant to epigenetic silencing. Synthetic modules need to be compatible with analogous properties of stem cells, and how these natural properties change during differentiation needs to be taken into consideration for long-term coupling experiments. The timing of coupling the signalling centre to the stem cell-derived aggregate is also critical, as signalling ligands often exert different roles depending on developmental context. Growth is another parameter that needs to be taken into account, due to its connection with patterning.[2,3,7] Lastly, while our method automates the generation of synthetic signalling centres, it produces variability in size and stoichiometry of EB-HEK co-aggregates, thus in the balance between endogenous and exogenous signalling. While this beneficially generates a wide range of novel phenotypes, co-aggregate standardization would require an inevitable increase in manual input.

Future Directions

The prototypic platform presented in this report provides proof-of-concept for creating spatially localized, organizer-like signalling centres that produce signals of the user's choice, to control facets of EB organization. This synthetic biology-inspired approach provides a novel method for the localized provision of signalling ligands from cell-based factories that self-organize with mESCs and EBs, and opens up interesting directions for future applications. During *in vivo* gastrulation, the anterior pole of the embryo expresses antagonists (*Dkk1, Lefty1, Cerl*)[8–10] whereas the posterior expresses agonists of signalling pathways (*Bmp4, Wnt3, Fgf8, Nodal* early on).[11–15,43] Based on such findings from embryo development, and utilizing the resource presented herein, it now becomes possible to engineer "inhibitory" and "activator" HEK^{Cdh3} organizers, apply them to opposite poles of differentiating EBs, and investigate how signalling controls self-organization in a bottom-up manner. This system puts us one step closer towards engineering *bona fide* synthetic organizers.

The problems that have plagued EB development are also challenges to the generation of more realistic organoids that represent specialized parts of mature embryos. Organoid development proceeds largely autonomously, with intercellular interactions controlling the separation of tissue-like compartments and the generation of fine-scale anatomy, but with little or no signs of organ-scale order that often entails asymmetry.[4,25,44–46] Imposing artificial symmetry breaking cues on organoids, for example by the manual placement of beads soaked in inductive factors,[47] can polarize their development and improve organ-scale anatomy but these approaches are time-consuming, limited in scalability, and yield highly variable results. For such reasons, engineering biological mechanisms to break the symmetry during organoid self-organization has drawn increasing interest in order to improve the realism in organoid anatomy.[48] For example, iPSCs engineered to produce SHH have been used to break symmetry and improve patterning in cerebral organoids, but because SHH-producing and wild-type iPSCs do not spontaneously self-organize, manual layering is required to localize SHH producers and even then heterotypic cells can intermingle, which creates efficiency issues.[28] The synthetic biology approach we present efficiently generates local signalling centres automatically. In the future, it will be interesting to test whether HEK^{Cdh3}-based centres can be used to apply polarizing activities and induce symmetry breaking in advanced stem cell-derived systems and organoids. For example, HEK$^{Cdh3\text{-}Wnt3a}$ have potential in organoid experimentation due to the critical role of WNT3A in organoid biology.[32,35,37,49] For such investigations, it would be critical that HEK^{Cdh3}-based lines are compatible with stable and long-term signalling and morphogenesis, which is supported by preliminary observations (Supplemental Figure 4). Ultimately, we primarily seek to demonstrate proof-of-concept that synthetic biology can be used to program naïve cells to behave as self-organizing signalling centres, which can influence fate decisions locally and control patterning in stem cell-derived 3D aggregates.

Materials and methods

Cell sourcing

Wild-type IB10 mESCs were sourced from the Dzierzak lab; *7xTCF/LEF::eGFP* mESCs from ref[17]; *T-brachyury::eGFP* mESCs from ref[38]. HEK^{Cdh3} and HEK^{Cdh1} were sourced from the Davies lab.[30] All "HEK" cells in this study are TREx-293-derived, which are HEK-293 cells stably expressing the tetracycline repressor TetR, allowing for tetracycline-inducible expression of TetO-regulated cadherin transgenes.

Cell culture

TREx-293/HEK cells were maintained in Dulbecco's modified Eagle medium (DMEM; Gibco #41966-052) supplemented with foetal bovine serum (FBS; 10%), L-glutamine (2mM; Gibco #25030-024), penicillin/streptomycin (pen/strep; 100U/ml; 100µg/ml; Gibco #15140-122) and blasticidin (5µg/ml). Cultures were passaged every 3-4 days, when at 80-90% confluence, in a 1:10-1:12 ratio. Mouse ESCs were maintained on irradiated mouse embryonic fibroblasts (MEFs; Amsbio #ASF-1201) in high glucose DMEM (Lonza #BE12-604F/U1) supplemented with HyClone FBS (15%; Healthcare #10309433, SV30160.03, Lot RB35954), GlutaMAX (2mM; Gibco #35050-038), sodium pyruvate (1mM; Gibco #11360-039), non-essential amino-acids (0.1mM; Lonza #BE13-114E), β-mercaptoethanol (0.1mM; Gibco #31350-010), pen/strep (100U/ml; 100µg/ml; Gibco #15140-122) and leukaemia inhibitory factor (LIF; 1000U/ml; Santa Cruz Biotechnology #sc-4989A). LIF was added fresh in complete medium aliquots weekly, and culture medium was replaced daily. Thawn MEFs were used for maximum 7 days, seeded at $2x10^6$ cells per well-plate, in mESC maintenance medium without LIF. ESC cultures were passaged every 2-3 days depending on colony size, in a 1:10 ratio.

Cell engineering

mCherry was amplified from *pCherryPickerControl* (Clontech) using forward primer (AGGCGTGTACGGTGGGAG) and reverse primer (CCGCATGTTAGAAGACTTCCTCTGCCCTCTCCTCCGGACCCGCCGCCTTTGTACAGCTCGTCCATGC). *Wnt3a* was amplified from NIH3T3-Wnt3a-derived cDNA using forward primer (GCAGAGGAAGTCTTCTAACATGCGGTGACGTGGAGGAGAATCCTGGCCCAATGGCTCCTCTCGGATACC) and reverse primer (GGGGACCACTTTGTACAAGAAAGCTGGGTCTACTTGCAGGTGTGCACG). *attB1-mCherry-2A* and *2A-Wnt3a-attB2* were joined into *attB1-mCherry-2A-Wnt3a-attB2* via Fusion PCR and shuttled

into *pDONR221* via Gateway cloning to create *pENTR-mCherry-2A-Wnt3a*. The *mCherry-2A-Wnt3a* cassette was moved from *pENTR* into *pSelexie(Hygro)-CMV-ccdB* via Gateway cloning. HEK^{Cdh3} grown on 6-wells were transfected with 1µg *pSelexie-CMV-mCherry-2A-Wnt3a* using Lipofectamine 3000 (ThermoFisher #L3000001) and selected using 450µg/ml hygromycin B (Sigma #10843555001) for 14 days. Single colonies were manually picked, expanded and tested for pattern formation with HEK^{Cdh1}.

Reporter activation assays

Culture medium of *7xTCF/LEF::eGFP* mESC 24h-cultures was replaced with mESC maintenance medium comprising CHIRON-99021 (5µM), human recombinant WNT3A (10nM; R&D Systems #5036-WN-010), 50% medium conditioned by HEK^{Cdh3} for 5 days, or 50% medium conditioned by HEK$^{Cdh3\text{-}Wnt3a}$ for 5 days. LIF was adjusted for dilutions of mESC maintenance medium with HEK-conditioned media.

Embryoid body differentiation

Trypsinized mESCs were resuspended in 5ml Iscove's modified Dulbecco's medium (IMDM; Gibco #21056-023) supplemented with 20% HyClone FBS and pen/strep, plated on 6cm-diameter dishes (Greiner Bio-One #628160), and incubated at 37ºC, 5% CO_2 for 30-40min. The supernatant was harvested and $7.5x10^4$ mESCs were resuspended in IMDM supplemented with HyClone FBS (15%), GlutaMAX (2mM), ascorbic acid (50µg/ml; Sigma #A4544-25G), transferrin (150µg/ml; Roche #10652202001) and monothioglycerol (39nl/ml; Sigma #M6145-25ML). Cells ($75x10^3$ mESCs in 3ml medium) were plated on a 6cm-diameter petri dish (VRW #391-0866) and incubated on a rotator platform at 40rpm, 37ºC, 5% CO_2. Medium was replaced at 72h of differentiation, and additionally comprised 5% protein-free hybridoma medium (5%; Gibco #12040-077). Samples were analysed at 96h of differentiation.

Pattern formation co-cultures

HEK^{Cdh3}/HEK$^{Cdh3\text{-}Wnt3a}$ and HEK^{Cdh1} cells were cultured in maintenance medium containing tetracycline (10µM) for 24h. Cells were harvested, mixed in a 1:2 ratio (HEK^{Cdh3}/HEK$^{Cdh3\text{-}Wnt3a}$ to HEK^{Cdh1}) and seeded at a density of $7.5\text{-}9.0x10^4$ cells/cm^2 in tetracycline-supplemented medium. For 3D cultures, $1\text{-}20x10^3$ cells were deposited on low-adhesion U-bottom 96-wells. For EBs experiments, $4x10^4$ tetracycline-stimulated HEK^{Cdh3}/HEK$^{Cdh3\text{-}Wnt3a}$ were added to petri dishes containing EBs at 24h of

differentiation, along with tetracycline (10μM). Tetracycline was included in the medium replacement at 72h of differentiation. For details see also Supplemental Figure 1.

Immunostaining

EBs were collected in 0.4ml medium and washed in 1ml PBS deposited in a 1.5ml Eppendorf tube. After aspiration, EBs were fixed in 0.6ml 4% paraformaldehyde and kept on ice for 1h, mixing at 30min. Samples were washed with 0.9ml PBS -0.5% TritonX-100 (PBT) for 30min, three times, and blocked with 0.5ml PBT -10% donkey serum for 2h as described elsewhere.[17] EBs were stained in 0.4ml PBS containing rabbit anti-GFP (1:500; MBL #598), mouse anti-mCherry (1:500; Novus Biologicals #NBP1-96752SS) and goat anti-Brachyury (1:500; R&D Systems #AF2085), at 4ºC overnight on a rocking platform. Staining solution was aspirated and samples were washed three times in PBS on ice. The staining-washing process was repeated with 0.4ml PBS containing 0.4μM DAPI, donkey anti-rabbit AlexaFluor488 (1:200; ThermoFisher #A21206), donkey anti-mouse AlexaFluor594 (1:200; ThermoFisher #A21203) and donkey anti-goat AlexaFluor647 (1:200; ThermoFisher #A21447). For antibodies, see also Supplemental Table 1.

Imaging

Stained EBs were dehydrated in 50% methanol for 10-15min, then 100% methanol for 10-15min, at 4ºC on a rocking platform. Clearing was performed in Eppendorf tubes mounted on glass scintillation vials using benzyl alcohol (Sigma #402834) benzyl benzoate (Sigma #B6630) (BABB; 1:2). EBs were cleared twice with 0.2ml of 50% BABB (50% methanol), then three times with 100% BABB, for 1-2min per wash. In 0.19ml BABB, EBs were transferred to a chamber made of FastWell frame (GraceBio-Labs #664113 FW20) and a 25mm-wide, 0.15mm-thick round coverslip (VWR #631-1584), which was sealed with another coverslip and glued to a SuperFrost Ultra Plus histology slide (ThermoScientific #10417002) as described elsewhere.[50] EBs were imaged on a Leica TCS SP8 laser scanning confocal microscope using x40 objective lens and oil.

Image processing

Images were processed using Fiji (https://fiji.sc/). Quantifications occurred at original/unedited files. For colony fluorescence quantification, the average background for each image was calculated based on 30μm-diameter circle measurements, placed on empty regions at three central areas and four corners of the image. Colony fluorescence was measured in 30μm-diameter circles placed on mESC colonies.

The average background was subtracted from each colony value of that image. For EB fluorescence quantification, grayscale values where determined in rectangular regions of interest. For presentation purposes, background was reduced by raising the minimum display limit value until no background was evident and as long as staining specificity did not change. The *Process->Noise->Despeckle* command was used where applicable. Whole EB images were composed through the *Image->Stacks->3D Project…* tool.

Flow cytometry

EBs were collected in 0.5ml medium and washed in 3ml PBS deposited in a 14ml Falcon tube. After aspiration, 1ml TrypLE Express (Gibco #12604-013) was added and samples were incubated at 37^{o}C (water bath) for 8-10min, shaking occasionally. Samples were mixed with 2ml flow buffer (PBS -10% heat-inactivated FBS) to aid dissociation, resuspended in 0.7ml flow buffer and filtered through flow cytometry tube cap filters (Falcon/Corning #352235). Hoechst viability dye was mixed in immediately prior to flow cytometry analysis. Post-capture data analysis was performed using FlowJo (https://www.flowjo.com/solutions/flowjo).

Supporting Information

Supplemental Figure 1 - 4 and Supplemental Table 1. Method overview; conditioned media experiments; flow cytometry gating; preliminary long-term coupling experiments; list of antibodies.

Author Contributions

F.G. designed and performed experiments, analysed the data, and wrote the manuscript. E.C. and I.B. constructed *pSelexie-CMV-mCherry-2A-Wnt3a*. E.D. and J.A.D. provided advice, supervision and co-wrote the manuscript.

Funding

This work was funded by the BBSRC's grant to the UK Centre for Mammalian Synthetic Biology, grant BB/M018040/1.

Competing interests

No competing interests declared.

Acknowledgements

We thank the Queen's Medical Research Institute flow cytometry and cell sorting facility for assistance with flow cytometry analyses, and the Queen's Medical Research Institute confocal and advanced light microscopy facility for assistance with confocal imaging (The University of Edinburgh). We thank Chris S. Vink (The University of Edinburgh) for technical guidance on clearing of biological samples, and Derk ten Berge (Erasmus Medical Center, Netherlands) for kindly providing *7xTCF/LEF::eGFP* mESCs and critical discussion of the manuscript.

Abbreviations

Bmp4: bone morphogenetic protein 4. Cdh1: E-cadherin. Cdh3: P-cadherin. Dkk1: Dickkopf-related protein 1. EB: embryoid body. mESC: (mouse) embryonic stem cell. Fgf8: fibroblast growth factor 8. GFP: green fluorescent protein. HEK: TREx-293 cells. HEK^{Cdh1}/HEK^{Cdh3}/$HEK^{Cdh3\text{-}Wnt3a}$: TREx-293

cells synthetically expressing Cdh1, Cdh3, or Cdh3 and Wnt3a genes. iPSC: induced pluripotent stem cell. R1$^{7xTCF/LEF::eGFP}$: mouse embryonic stem cells reporting Wnt/β-catenin activity via enhanced GFP. SHH: sonic hedgehog. T-brachyury::eGFP: reporting T-brachyury expression via enhanced GFP. TetR: tetracycline repressor. TREx-293: human embryonic kidney 293 cells stably expressing TetR.

References

(1) Shahbazi, M. N., Siggia, E. D., and Zernicka-Goetz, M. (2019) Self-organization of stem cells into embryos: A window on early mammalian development. *Science 364*, 948–951.

(2) Lander, A. D. (2011) Pattern, growth, and control. *Cell 144*, 955–969.

(3) Davies, J. A., and Glykofrydis, F. (2020) Engineering pattern formation and morphogenesis. *Biochem Soc Trans 48*, 1177–1185.

(4) Davies, J. A. (2018) Adaptive self-organization in the embryo: its importance to adult anatomy and to tissue engineering. *J Anat 232*, 524–533.

(5) Martinez Arias, A., and Steventon, B. (2018) On the nature and function of organizers. *Development 145*.

(6) Wolpert, L. (1969) Positional information and the spatial pattern of cellular differentiation. *J Theor Biol 25*, 1–47.

(7) Kicheva, A., and Briscoe, J. (2015) Developmental Pattern Formation in Phases. *Trends Cell Biol 25*, 579–591.

(8) Yamamoto, M., Saijoh, Y., Perea-Gomez, A., Shawlot, W., Behringer, R. R., Ang, S.-L., Hamada, H., and Meno, C. (2004) Nodal antagonists regulate formation of the anteroposterior axis of the mouse embryo. *Nature 428*, 387–392.

(9) Perea-Gomez, A., Vella, F. D. J., Shawlot, W., Oulad-Abdelghani, M., Chazaud, C., Meno, C., Pfister, V., Chen, L., Robertson, E., Hamada, H., Behringer, R. R., and Ang, S.-L. (2002) Nodal antagonists in the anterior visceral endoderm prevent the formation of multiple primitive streaks. *Dev Cell 3*, 745–756.

(10) Lewis, S. L., Khoo, P.-L., De Young, R. A., Steiner, K., Wilcock, C., Mukhopadhyay, M., Westphal, H., Jamieson, R. V., Robb, L., and Tam, P. P. L. (2008) Dkk1 and Wnt3 interact to control head morphogenesis in the mouse. *Development 135*, 1791–1801.

(11) Rivera-Pérez, J. A., and Magnuson, T. (2005) Primitive streak formation in mice is preceded by localized activation of Brachyury and Wnt3. *Dev Biol 288*, 363–371.

(12) Brennan, J., Lu, C. C., Norris, D. P., Rodriguez, T. A., Beddington, R. S., and Robertson, E. J. (2001) Nodal signalling in the epiblast patterns the early mouse embryo. *Nature 411*, 965–969.

(13) Ben-Haim, N., Lu, C., Guzman-Ayala, M., Pescatore, L., Mesnard, D., Bischofberger, M., Naef, F., Robertson, E. J., and Constam, D. B. (2006) The nodal precursor acting via activin receptors induces mesoderm by maintaining a source of its convertases and BMP4. *Dev Cell 11*, 313–323.

(14) Di-Gregorio, A., Sancho, M., Stuckey, D. W., Crompton, L. A., Godwin, J., Mishina, Y., and Rodriguez, T. A. (2007) BMP signalling inhibits premature neural differentiation in the mouse embryo. *Development 134*, 3359–3369.

(15) Dunn, N. R., Vincent, S. D., Oxburgh, L., Robertson, E. J., and Bikoff, E. K. (2004) Combinatorial activities of Smad2 and Smad3 regulate mesoderm formation and patterning in the mouse embryo. *Development 131*, 1717–1728.

(16) Bardot, E. S., and Hadjantonakis, A.-K. (2020) Mouse gastrulation: Coordination of tissue patterning, specification and diversification of cell fate. *Mech Dev 163*, 103617.

(17) ten Berge, D., Koole, W., Fuerer, C., Fish, M., Eroglu, E., and Nusse, R. (2008) Wnt signaling mediates self-organization and axis formation in embryoid bodies. *Cell Stem Cell 3*, 508–518.

(18) van den Brink, S. C., Baillie-Johnson, P., Balayo, T., Hadjantonakis, A.-K., Nowotschin, S., Turner, D. A., and Martinez Arias, A. (2014) Symmetry breaking, germ layer specification and axial organisation in aggregates of mouse embryonic stem cells. *Development 141*, 4231–4242.

(19) Beccari, L., Moris, N., Girgin, M., Turner, D. A., Baillie-Johnson, P., Cossy, A.-C., Lutolf, M. P., Duboule, D., and Arias, A. M. (2018) Multi-axial self-organization properties of mouse embryonic stem cells into gastruloids. *Nature 562*, 272–276.

(20) Turner, D. A., Girgin, M., Alonso-Crisostomo, L., Trivedi, V., Baillie-Johnson, P., Glodowski, C. R., Hayward, P. C., Collignon, J., Gustavsen, C., Serup, P., Steventon, B., P Lutolf, M., and Arias, A. M. (2017) Anteroposterior polarity and elongation in the absence of extra-embryonic tissues and of spatially localised signalling in gastruloids: mammalian embryonic organoids. *Development 144*, 3894–3906.

(21) Warmflash, A., Sorre, B., Etoc, F., Siggia, E. D., and Brivanlou, A. H. (2014) A method to recapitulate early embryonic spatial patterning in human embryonic stem cells. *Nat Methods 11*, 847–854.

(22) Tewary, M., Ostblom, J., Prochazka, L., Zulueta-Coarasa, T., Shakiba, N., Fernandez-Gonzalez, R., and Zandstra, P. W. (2017) A stepwise model of reaction-diffusion and positional information governs self-organized human peri-gastrulation-like patterning. *Development 144*, 4298–4312.

(23) Manfrin, A., Tabata, Y., Paquet, E. R., Vuaridel, A. R., Rivest, F. R., Naef, F., and Lutolf, M. P. (2019) Engineered signaling centers for the spatially controlled patterning of human pluripotent stem cells. *Nat Methods 16*, 640–648.

(24) Guye, P., Ebrahimkhani, M. R., Kipniss, N., Velazquez, J. J., Schoenfeld, E., Kiani, S., Griffith, L. G., and Weiss, R. (2016) Genetically engineering self-organization of human pluripotent stem cells into a liver bud-like tissue using Gata6. *Nat Commun 7*, 10243.

(25) Antonica, F., Kasprzyk, D. F., Opitz, R., Iacovino, M., Liao, X.-H., Dumitrescu, A. M., Refetoff, S., Peremans, K., Manto, M., Kyba, M., and Costagliola, S. (2012) Generation of functional thyroid from embryonic stem cells. *Nature 491*, 66–71.

(26) Amadei, G., Lau, K. Y. C., De Jonghe, J., Gantner, C. W., Sozen, B., Chan, C., Zhu, M., Kyprianou, C., Hollfelder, F., and Zernicka-Goetz, M. (2021) Inducible Stem-Cell-Derived Embryos Capture Mouse Morphogenetic Events In Vitro. *Dev Cell 56*, 366-382.e9.

(27) Sagy, N., Slovin, S., Allalouf, M., Pour, M., Savyon, G., Boxman, J., and Nachman, I. (2019) Prediction and control of symmetry breaking in embryoid bodies by environment and signal integration. *Development 146*.

(28) Cederquist, G. Y., Asciolla, J. J., Tchieu, J., Walsh, R. M., Cornacchia, D., Resh, M. D., and Studer, L. (2019) Specification of positional identity in forebrain organoids. *Nat Biotechnol 37*, 436–444.

(29) Foty, R. A., and Steinberg, M. S. (2005) The differential adhesion hypothesis: a direct evaluation. *Dev Biol 278*, 255–263.

(30) Cachat, E., Liu, W., Martin, K. C., Yuan, X., Yin, H., Hohenstein, P., and Davies, J. A. (2016) 2- and 3-dimensional synthetic large-scale de novo patterning by mammalian cells through phase separation. *Sci Rep 6*, 20664.

(31) Pieters, T., and van Roy, F. (2014) Role of cell-cell adhesion complexes in embryonic stem cell biology. *J Cell Sci 127*, 2603–2613.

(32) Willert, K., Brown, J. D., Danenberg, E., Duncan, A. W., Weissman, I. L., Reya, T., Yates, J. R., and Nusse, R. (2003) Wnt proteins are lipid-modified and can act as stem cell growth factors. *Nature 423*, 448–452.

(33) Takada, R., Mii, Y., Krayukhina, E., Maruyama, Y., Mio, K., Sasaki, Y., Shinkawa, T., Pack, C.-G., Sako, Y., Sato, C., Uchiyama, S., and Takada, S. (2018) Assembly of protein complexes restricts diffusion of Wnt3a proteins. *Commun Biol 1*, 165.

(34) Yamaguchi, T. P., Takada, S., Yoshikawa, Y., Wu, N., and McMahon, A. P. (1999) T (Brachyury) is a direct target of Wnt3a during paraxial mesoderm specification. *Genes Dev 13*, 3185–3190.

(35) Tüysüz, N., van Bloois, L., van den Brink, S., Begthel, H., Verstegen, M. M. A., Cruz, L. J., Hui, L., van der Laan, L. J. W., de Jonge, J., Vries, R., Braakman, E., Mastrobattista, E., Cornelissen, J. J., Clevers, H., and Ten Berge, D. (2017) Lipid-mediated Wnt protein stabilization enables serum-free culture of human organ stem cells. *Nat Commun 8*, 14578.

(36) Lowndes, M., Rotherham, M., Price, J. C., El Haj, A. J., and Habib, S. J. (2016) Immobilized WNT Proteins Act as a Stem Cell Niche for Tissue Engineering. *Stem Cell Reports 7*, 126–137.

(37) Farin, H. F., Jordens, I., Mosa, M. H., Basak, O., Korving, J., Tauriello, D. V. F., de Punder, K., Angers, S., Peters, P. J., Maurice, M. M., and Clevers, H. (2016) Visualization of a short-range Wnt gradient in the intestinal stem-cell niche. *Nature 530*, 340–343.

(38) Fehling, H. J., Lacaud, G., Kubo, A., Kennedy, M., Robertson, S., Keller, G., and Kouskoff, V. (2003) Tracking mesoderm induction and its specification to the hemangioblast during embryonic stem cell differentiation. *Development 130*, 4217–4227.

(39) Etoc, F., Metzger, J., Ruzo, A., Kirst, C., Yoney, A., Ozair, M. Z., Brivanlou, A. H., and Siggia, E. D. (2016) A Balance between Secreted Inhibitors and Edge Sensing Controls Gastruloid Self-Organization. *Dev Cell 39*, 302–315.

(40) Britton, G., Heemskerk, I., Hodge, R., Qutub, A. A., and Warmflash, A. (2019) A novel self-organizing embryonic stem cell system reveals signaling logic underlying the patterning of human ectoderm. *Development 146*.

(41) Heemskerk, I., Burt, K., Miller, M., Chhabra, S., Guerra, M. C., Liu, L., and Warmflash, A. (2019) Rapid changes in morphogen concentration control self-organized patterning in human embryonic stem cells. *Elife 8*.

(42) Habib, S. J., Chen, B.-C., Tsai, F.-C., Anastassiadis, K., Meyer, T., Betzig, E., and Nusse, R. (2013) A localized Wnt signal orients asymmetric stem cell division in vitro. *Science 339*, 1445–1448.

(43) Ciruna, B., and Rossant, J. (2001) FGF signaling regulates mesoderm cell fate specification and morphogenetic movement at the primitive streak. *Dev Cell 1*, 37–49.

(44) Renner, M., Lancaster, M. A., Bian, S., Choi, H., Ku, T., Peer, A., Chung, K., and Knoblich, J. A. (2017) Self-organized developmental patterning and differentiation in cerebral organoids. *EMBO J 36*, 1316–1329.

(45) Serra, D., Mayr, U., Boni, A., Lukonin, I., Rempfler, M., Challet Meylan, L., Stadler, M. B., Strnad, P., Papasaikas, P., Vischi, D., Waldt, A., Roma, G., and Liberali, P. (2019) Self-organization and symmetry breaking in intestinal organoid development. *Nature 569*, 66–72.

(46) Takata, N., Sakakura, E., Eiraku, M., Kasukawa, T., and Sasai, Y. (2017) Self-patterning of rostral-caudal neuroectoderm requires dual role of Fgf signaling for localized Wnt antagonism. *Nat Commun 8*, 1339.

(47) Mills, C. G., Lawrence, M. L., Munro, D. A. D., Elhendawi, M., Mullins, J. J., and Davies, J. A. (2017) Asymmetric BMP4 signalling improves the realism of kidney organoids. *Sci Rep 7*, 14824.

(48) Brassard, J. A., and Lutolf, M. P. (2019) Engineering Stem Cell Self-organization to Build Better Organoids. *Cell Stem Cell 24*, 860–876.

(49) Shin, W., Wu, A., Min, S., Shin, Y. C., Fleming, R. Y. D., Eckhardt, S. G., and Kim, H. J. (2020) Spatiotemporal Gradient and Instability of Wnt Induce Heterogeneous Growth and Differentiation of Human Intestinal Organoids. *iScience 23*, 101372.

(50) Yokomizo, T., Yamada-Inagawa, T., Yzaguirre, A. D., Chen, M. J., Speck, N. A., and Dzierzak, E. (2012) Whole-mount three-dimensional imaging of internally localized immunostained cells within mouse embryos. *Nat Protoc 7*, 421–431.